Available online at www.sciencedirect.com

ScienceDirect

Geochimica et Cosmochimica Acta 220 (2018) 291–308

Geochimica et Cosmochimica Acta

www.elsevier.com/locate/gca

Modeling uranium(VI) adsorption onto montmorillonite under varying carbonate concentrations: A surface complexation model accounting for the spillover effect on surface potential

C. Tournassat [a,b,*], R.M. Tinnacher [b,c], S. Grangeon [d], J.A. Davis [b]

[a] UMR 7327 Institut des Sciences de la Terre d'Orléans (ISTO), Université d'Orléans–CNRS/INSU–BRGM, Orléans, France
[b] Earth and Environmental Sciences Area, Lawrence Berkeley National Laboratory, Berkeley, CA 94720, USA
[c] Department of Chemistry & Biochemistry, California State University East Bay, Hayward, CA 94542, USA
[d] BRGM, French Geological Survey, Orléans, France

Received 2 February 2017; accepted in revised form 26 September 2017; Available online 6 October 2017

Abstract

The prediction of U(VI) adsorption onto montmorillonite clay is confounded by the complexities of: (1) the montmorillonite structure in terms of adsorption sites on basal and edge surfaces, and the complex interactions between the electrical double layers at these surfaces, and (2) U(VI) solution speciation, which can include cationic, anionic and neutral species. Previous U(VI)-montmorillonite adsorption and modeling studies have typically expanded classical surface complexation modeling approaches, initially developed for simple oxides, to include both cation exchange and surface complexation reactions. However, previous models have not taken into account the unique characteristics of electrostatic surface potentials that occur at montmorillonite edge sites, where the electrostatic surface potential of basal plane cation exchange sites influences the surface potential of neighboring edge sites ('spillover' effect).

A series of U(VI) – Na-montmorillonite batch adsorption experiments was conducted as a function of pH, with variable U(VI), Ca, and dissolved carbonate concentrations. Based on the experimental data, a new type of surface complexation model (SCM) was developed for montmorillonite, that specifically accounts for the spillover effect using the edge surface speciation model by Tournassat et al. (2016a). The SCM allows for a prediction of U(VI) adsorption under varying chemical conditions with a minimum number of fitting parameters, not only for our own experimental results, but also for a number of published data sets. The model agreed well with many of these datasets without introducing a second site type or including the formation of ternary U(VI)-carbonato surface complexes. The model predictions were greatly impacted by utilizing analytical measurements of dissolved inorganic carbon (DIC) concentrations in individual sample solutions rather than assuming solution equilibration with a specific partial pressure of CO_2, even when the gas phase was laboratory air. Because of strong aqueous U(VI)-carbonate solution complexes, the measurement of DIC concentrations was even important for systems set up in the 'absence' of CO_2, due to low levels of CO_2 contamination during the experiment.

Keywords: Uranium; Adsorption; Clay; Montmorilonite; Spillover; Surface complexation modeling

* Corresponding author at: UMR 7327 Institut des Sciences de la Terre d'Orléans (ISTO), Université d'Orléans–CNRS/INSU–BRGM, Orléans, France.
E-mail address: c.tournassat@brgm.fr (C. Tournassat).

https://doi.org/10.1016/j.gca.2017.09.049
0016-7037/Published by Elsevier Ltd.

1. INTRODUCTION

Due to mining, milling and fuel processing operations, numerous sites have been contaminated with uranium in the past, with 38 proposed or final Superfund sites on the EPA National Priority List in the U.S. alone (NIH, 2016). In the future, the long-term storage of nuclear waste has the potential to create additional sources of uranium contamination affecting subsurface environments and drinking water resources. Chemically-induced, acute effects of uranium in humans, such as an inflammation of the kidneys (nephritis), have been reported (Hursh and Spoor, 1973), while chronic health effects and carcinogenicity are less well understood (World Health Organization, 2004). At this point in time, the World Health Organization has proposed a provisional guideline value of 15 μg $U{\cdot}L^{-1}$ in drinking water (World Health Organization, 2004); the current U.S. EPA Maximum Contaminant Level (MCL) is set at 30 μg $U{\cdot}L^{-1}$ (U.S. Environmental Protection Agency, 2001). A sound scientific understanding of uranium mobility is needed in order to evaluate risks to humans and the environment, to optimize the management of nuclear waste and to take appropriate remediation actions if necessary.

The most relevant factors controlling uranium transport in saturated porous media are uranium solubility in pore water solutions and uranium adsorption reactions to mineral surfaces. Uranium can exist at oxidation states of IV or VI, but U(VI) is the most relevant oxidation state in most surface waters and in oxic groundwaters (Choppin, 2006). In reducing environments, the low solubility of U(IV) mineral phases greatly decreases uranium mobility.

Numerous studies have demonstrated the impacts of pH, bicarbonate and calcium concentrations on U(VI) solution speciation, adsorption and transport behavior (Davis et al., 2004; Curtis et al., 2004; Fox et al., 2006; Hartmann et al., 2008). Potential changes in chemical solution conditions and contaminant solution speciation over time and space are especially relevant for uranium, given the long half-lives of uranium isotopes and complex transport pathways in engineered systems and the natural environment. For instance, in nuclear waste repositories, pore water pH is buffered at values between 7 and 8 in the bentonite backfill material of engineered barrier systems surrounding waste canisters and/or in the clay host-rock (Muurinen and Lehikoinen, 1999; Bradbury and Baeyens, 2003; Wersin, 2003; Wersin et al., 2004; Tournassat et al., 2015c). However, more alkaline pH conditions are expected in close proximity to steel canisters (pH 8–11) due to corrosion processes (Bildstein and Claret, 2015), as well as in cementitious leachates at bentonite-concrete boundaries (pH > 13 for Ordinary Portland Cement and pH 9–11 for low alkali cement) due to the chemical degradation of cement (Savage et al., 1992; Gaucher and Blanc, 2006; Gaboreau et al., 2012b; Milodowski et al., 2016). Furthermore, dissolved calcium concentrations may also vary over time and space due to the progressive degradation of cement-based engineered barriers, the specific calcite contents in clay host rocks or changing concentrations in carbonate minerals along transport pathways (Hartmann et al., 2008; Gaboreau et al., 2012a; Adinarayana et al., 2013).

These chemical gradients in waste scenarios are important for the fate and transport of uranium, since U(VI) aqueous speciation is very complex. For instance, the uranyl cation (UO_2^{2+}) typically dominates speciation at low pH, while neutral and anionic U(VI)-hydroxyl and carbonate complexes become predominant at higher pH conditions. In a dilute U(VI) solution at pH 7 in the absence of carbonate, the predominant U(VI) species is the neutral $UO_2(OH)_2^0$. In comparison, for the same solution in equilibrium with atmospheric CO_2, the predominant species is the anion $(UO_2)_2CO_3(OH)_3^-$ (for a 1 μmol·L^{-1} solution). However, groundwater solutions are typically in equilibrium with partial pressures of CO_2 (pCO_2) at 1 % or greater, and may contain considerable concentrations of calcium due to the presence of carbonate minerals. At 1 % pCO_2, pH 7 and in the *absence* of Ca, U(VI) solution speciation is dominated by the anion $UO_2(CO_3)_2^{2-}$ (Fig. EA-1, Electronic Annex). For a comparable solution in equilibrium with calcite, the predominant U(VI) species is the neutral $Ca_2UO_2(CO_3)_3^0$ (Fig. EA-2, Electronic Annex).

Clay minerals are important minerals to consider in uranium contaminant transport because of the proposed use of bentonite or clay-rocks as a buffer material in engineered and natural barrier systems at future nuclear waste disposal sites (Tournassat et al., 2015b). Furthermore, there is the possibility that colloid-facilitated transport of uranium adsorbed on clay or bentonite particles may occur near granite waste repositories (Geckeis et al., 2004; Schäfer et al., 2004; Missana et al., 2008). Last, clay contents in soils and sediments are often high at uranium-contaminated sites (Grawunder et al., 2009; Graham et al., 2011).

Sodium-montmorillonite is the focus of this study because this mineral is the major component of bentonite in barrier systems. Montmorillonite is a smectite, a 2:1-layer-type dioctahedral phyllosilicate with a large specific surface area (~750 $m^2{\cdot}g^{-1}$) and cation exchange capacity (~1 $mol_c{\cdot}kg^{-1}$). Each montmorillonite layer has a thickness of ~1 nm and carries negative surface charges due to isomorphic substitutions of Al(III) for Si(IV) and Mg(II)/Fe(II) for Al(III) in its phyllosilicate framework (Brigatti et al., 2013). Due to its crystal structure, montmorillonite provides two types of surfaces and surface site types: (1) cation exchange sites, with a permanent surface charge, on basal planar surfaces, and (2) surface complexation sites, with variable surface charges as a function of pH, on edge surfaces of clay particles (Borisover and Davis, 2015).

Many research groups have investigated the surface speciation of adsorbed U(VI) on montmorillonite with EXAFS spectroscopy (Dent et al., 1992; Chisholm-Brause et al., 1994; Giaquinta et al., 1997; Sylwester et al., 2000; Hennig et al., 2002; Catalano and Brown, 2005; Schlegel and Descostes, 2009; Marques Fernandes et al., 2012; Troyer et al., 2016). Analysis of the data obtained at various ionic strengths reveals the presence of U(VI) outer-sphere complexes at low pH and/or low ionic strengths, and of U(VI) inner-sphere complexes at other conditions. These interpretations of EXAFS data are in qualitative agreement with the duality of adsorption mechanisms on montmorillonite surfaces, i.e. cation exchange on basal planar surfaces at low pH/ionic strength and surface

complexation on edge surfaces at other conditions, as also evinced by other spectrometric techniques for a range of different specifically adsorbed cations (Morris et al., 1994; Chisholm-Brause et al., 2001; Kowal-Fouchard et al., 2004; Wolthers et al., 2006).

The formation of inner-sphere bonds of U(VI) with surface groups at montmorillonite edge sites at neutral pH and high ionic strength was deduced from the splitting of the U(VI) oxygen equatorial shell into two distinct contributions at ~2.3 Å and ~2.5 Å in EXAFS spectra. However, there is considerable uncertainty in the interpretation of second neighbor atoms involved in these surface complexes. Hennig et al. (2002) concluded that surface mononuclear bidentate complexes formed at aluminol sites. Schlegel and Descostes (2009) also proposed a U-Al shell, in agreement with Hennig et al. (2002). Additional Polarized-EXAFS (P-EXAFS) characterizations allowed them to conclude that the U complex was located on the particle edges and corresponded to a mononuclear bidentate complex. In contrast, Catalano and Brown (2005) suggested that the primary surface group second neighbors were Fe atoms, where Fe has substituted for Al in the octahedral sheets. In addition, Catalano and Brown (2005) fitted their data with a U-C shell and suggested that ternary uranyl-carbonato species formed at the surface in the presence of carbonate. However, more recently, Marques Fernandes et al. (2012) and Troyer et al. (2016) concluded that it was not possible to conclusively distinguish between Fe, Al, and Si as second neighbor atoms in U(VI) EXAFS spectra. Furthermore, Marques Fernandes et al. (2012) did not find spectroscopic evidence for uranyl-carbonato complexes at the montmorillonite surface, despite the fact that their surface complexation model included the species. Troyer et al. (2016) were not able to confirm the presence of ternary uranyl-carbonato surface complexes from their EXAFS data either, but made a strong conclusion about the presence of such species from laser-induced fluorescence spectroscopy (LIFS) data. The LIFS results, however, were obtained at very high U(VI) equilibrium concentrations and high U(VI)/clay ratios. The total U(VI) concentration was 100 $\mu mol \cdot L^{-1}$ and solid-to-liquid ratio was 0.2 $g \cdot L^{-1}$, leading to an equilibrium U(VI) solution concentration of ~70 $\mu mol \cdot L^{-1}$. Although it is not known, these conditions might have favored the formation of uranyl carbonate complexes driven by a high total uranium-carbonate ratio.

An accurate prediction of uranium mobility in clay-rich environments is dependent upon the development of adsorption models that can capture: (1) the complex uranium solution and surface speciation as a function of chemical solution conditions, and (2) the complexity of montmorillonite and its implications for the conceptual description of adsorption processes. Surface complexation models (SCMs) have the ability to directly link U(VI) adsorption behavior with U(VI) solution speciation based on existing thermodynamic data, which allows the models to predict changes in adsorption as a function of chemical solution conditions over time and space. Several research groups have developed surface complexation models (SCMs) for the U(VI)-montmorillonite system (Pabalan and Turner, 1996; Turner et al., 1996; Hyun et al., 2001; Bradbury and Baeyens, 2005, 2011; Marques Fernandes et al., 2012). Surface complexation modeling studies predict that U(VI) adsorption decreases at alkaline pH when carbonate anions are present, due to the formation of strong aqueous uranyl-carbonato complexes (see Fig. EA-1, and see the aqueous speciation diagrams in Davis et al. (2004) and Fox et al. (2006)). However, the impact of the aqueous carbonate complexes on U(VI) sorption depends on whether these complexes adsorb on the clay surfaces or not. For example, in the model of Marques Fernandes et al. (2012), the authors found it necessary to include ternary uranyl-carbonato surface complexes to describe U(VI) adsorption onto montmorillonite in the presence of various concentrations of aqueous carbonate. Analogous U(VI) surface species have also been proposed on iron oxides and imogolite (Waite et al., 1994; Villalobos et al., 2001; Arai et al., 2007). For U(VI) adsorption on montmorillonite, however, in the absence of clear spectroscopic evidence, the need to add such additional surface complexes was guided by the quality of the fit between the model and the data. This fitting criterion may however be impaired by inadequate hypotheses in the modeling exercise. For example, the model of Marques Fernandes et al. (2012) was a non-electrostatic model, which means that the ionic nature of the sorbent and its interaction with the electrostatic potential field surrounding the montmorillonite particles is inherently not included. Given the complex U(VI) solution speciation described above, it is important to take into account that the interactions of cationic, neutral or anionic U(VI) solution species with the surface electrostatic field is influenced by their charge. Hence, an electrostatic model is needed in order to test the importance of the electrostatic interactions in quantifying U(VI) adsorption. Furthermore, the electrostatic model is needed to test whether it is necessary to include ternary uranyl-carbonato surface complexes in the model.

Currently available electrostatic surface complexation models for montmorillonite have been mostly based on the classical surface complexation models for oxides. These models are based on the hypothesis that surface charges are homogeneously distributed on a flat and infinite surface, which is an invalid assumption for clay minerals for the following two reasons. First, the edge surface is very different from a flat infinite surface in terms of its dimensions: while its length could be considered to be infinite, its width is always limited to 1 nm for individual layers dispersed in an electrolytic solution. Second, the surface potential developed by the permanent charges of the basal surfaces interacts with the surface potential at the edge surfaces with pH-dependent charge (Secor and Radke, 1985; Chang and Sposito, 1994; Bourg et al., 2007; Tournassat et al., 2013, 2015a, 2016a). This unique feature, called the spillover effect, must be taken into account in the development of an electrostatic model for montmorillonite edge surfaces.

Given the current uncertainties associated with results from spectroscopic studies and the modeling needs described above, the goals of this study are:

(1) to improve the current mechanistic understanding of uranium(VI) adsorption onto montmorillonite as a function of chemical conditions, with a specific focus on the role of dissolved inorganic carbon; and

(2) to develop an electrostatic surface complexation model that accounts for the impacts of the electric-double-layer (EDL) spillover effect on U(VI) surface reactions.

2. MATERIALS AND METHODS

For the development of U(VI) surface complexation models, it is important to carefully characterize the compositions of experimental solutions, because various other solutes may affect U(VI) solution or surface speciation. Uranium(VI) adsorption onto Na-montmorillonite was investigated here as a function of total U(VI), dissolved carbonate, and calcium concentrations (Table 1). Experimental blanks, standards and sample suspensions were analyzed for U(VI), calcium and dissolved inorganic carbon (DIC), and monitored for elements that could indicate clay dissolution or inadequate solid-liquid phase separation (for U(VI) and Ca background values, see Electronic Annex; Si, Al, Fe, K, and Mg data not reported). In addition, analytical detection limits and experimental background values for DIC solution concentrations were determined as described in further detail below. Analysis of DIC concentrations in supernatant solutions was of particular importance in our experiments, given the relevance of carbonate for U(VI) speciation.

2.1. Materials

Glassware was cleaned by soaking in acid (10 % (v/v) HCl) over 12–24 h, followed by thorough rinsing with Nanopure water and air-drying. All aqueous solutions were prepared with Nanopure water (Barnstead ultrapure water system) using chemicals of reagent grade or better. Acids, bases and salt solutions used in adsorption experiments were of TraceSelect grade (Sigma Aldrich), in order to minimize calcium background concentrations in particular. Uranium(VI) solutions contained U-238, either from an in-house or a commercially available uranyl nitrate stock solution (1.30 $mmol \cdot L^{-1}$ stock provided by Drs. David Singer and Wayne Lukens at Lawrence Berkeley National Laboratory, or various dilutions of a 1000 mg $U \cdot L^{-1}$ Inorganic Ventures ICP-MS standard).

A well-characterized, standardized source clay (Na-montmorillonite, SWy-2, Clay Minerals Society) was selected as the sorbent. Since this material is known to contain considerable impurities of quartz (8 %), feldspars (16 %) and calcite (Chipera and Bish, 2001; Costanzo and Guggenheim, 2001; Mermut and Cano, 2001), it was pretreated to avoid uncontrolled impacts of calcite dissolution on U(VI) solution speciation during adsorption experiments. The major purification steps, which have been described in detail elsewhere (Tinnacher et al., 2016), included: (1) dissolution of calcite impurities in 1 $mol \cdot L^{-1}$ sodium acetate/0.564 $mol \cdot L^{-1}$ acetic acid solution at pH 5, (2) conversion of the clay into its Na form, (3) separation of quartz and feldspar impurities from the <2 μm clay fraction by centrifugation, and (4) oven-drying of the clay mineral phase at 45 °C. Afterwards, clay stock suspensions of 10 or 20 $g \cdot L^{-1}$ were prepared in Nanopure water, and exact solid concentrations determined by weighing volume fractions before and after drying at 45 °C.

2.2. Experimental protocol for batch adsorption experiments

Uranium(VI) adsorption onto Na-montmorillonite was characterized as a function of pH, and total U(VI), DIC, and calcium concentrations (Table 1).

Batch adsorption experiments were conducted at room temperature (22.5–23.5 °C) at an ionic strength of 0.1, and a Na-montmorillonite concentration of 0.5 $g \cdot L^{-1}$ (except for experiment 7 with a solid concentration, m_s, of 0.24 $g \cdot L^{-1}$). pH values ranged from 3.9 to 10.2. The reaction time was 48.5 h, which closely approached or was sufficient to reach steady-state conditions (see discussion of kinetic adsorption data in the Electronic Annex). This reaction time is comparable to reaction times of 20–72 h used in other, similar studies (Chisholm-Brause et al., 1994; Hyun et al., 2001; Bradbury and Baeyens, 2005; Schlegel and Descostes, 2009). Total calcium concentrations varied from low micromolar background concentrations (see Electronic Annex) to the higher concentration of 2.1 $mmol \cdot L^{-1}$ in the experiment with added Ca.

The main steps in the batch adsorption experiments were: (1) pre-equilibration of Na-montmorillonite with a background electrolyte solution at specific pH and chemical solution conditions, (2) U(VI) adsorption equilibration with the mineral phase, and (3) sampling and analysis of supernatant fractions after removal of the solid phase by centrifugation. In the initial preparation of the solution/-clay suspensions, aliquots of Nanopure water,

Table 1
Experimental conditions for U(VI) batch adsorption experiments.

Expt. #	Range of pH	Total U(VI) conc. ($\mu mol \cdot L^{-1}$)	Range of dissolved inorganic carbon (DIC) ($mmol \cdot L^{-1}$)	Range of Ca ($\mu mol \cdot L^{-1}$)[a]
1	4.1–9.0	0.11	0.023–5.62	6.7–8.5
2	4.0–10.0	0.96	0.01–72	6.4–1.9
3	4.2–9.0	2.6	0.025–5.15	9.1–13
4	4.0–8.0	0.98	0.013–0.87	2100
5	3.9–9.9	1.1	0.0082–0.062	7.7–9.8
6	4.0–10.2	0.81	0.31–127	10–27
7	4.0–8.3	0.98	0.026–34.4	10–13

[a] Ca conc. in exp. 1–3 and 5–7 represent background values without any Ca additions (see Electronic Annex for details).

Na-montmorillonite stock suspension, 1 M NaCl and 0.1 M $CaCl_2$ solutions, and 1 M or 0.1 M $NaHCO_3$ solution were transferred into 50 mL polycarbonate centrifuge vials to yield the intended solid concentrations and aqueous compositions in the final sample volumes. The polycarbonate vials ('Oakridge centrifuge tubes') were chosen as sample vials to minimize U(VI) wall adsorption effects. The pH values were then adjusted to the intended values for the adsorption experiments with small volumes of HCl or NaOH.

During this initial preparation procedure, the solutions were exposed to one of three different gas phases: (1) atmospheric CO_2 in laboratory air (~0.04 %, 400 ppm), (2) CO_2-"free" atmosphere (in a glove box, filled with 94.3 % N_2/5.7 % H_2 gas mixture) and (3) elevated CO_2 atmospheres (intended to be 2 % CO_2/98 % N_2). In the CO_2-"free" experiment, the initial solutions used N_2-purged Nanopure water and were prepared in an anaerobic glove box purged with a 94.3 % N_2/5.7 % H_2 gas mixture. Two experiments involved exposure to elevated CO_2 atmospheres. In Experiment 6, the solutions were prepared in a disposable Sigma Aldrich glove bag purged with a 2 % CO_2/98 % N_2 gas mixture, but it was found subsequently that the purging of the glove bag was incomplete to remove all air (see Experimental Results section). Solutions in Experiment 7 were exposed in a COY glove box to the same gas mixture, but again it was found after the experiments that the glove box had been insufficiently purged with the gas mixture. After the preparation of the solutions, they were generally pre-equilibrated in closed sample vials by shaking for 12–24 h; however, in the case of Experiment 7 the vials were left open and exposed to the glove box atmosphere for 15 h.

After pre-equilibration with the electrolyte solution, aliquots of acidified U(VI) stock solution were added to obtain the intended total U(VI) concentrations in the experiments. Because the U(VI) stock solution was acidic, it was necessary to add small amounts of NaOH immediately following the U (VI) addition to adjust the pH to the intended experimental value. The vials were then shaken for 48.5 h. Afterwards, final pH values were recorded while minimizing gas exchange during the pH measurement (discussed further below). The sample suspensions were centrifuged to remove particles larger than approximately 50 nm from solution, as calculated based on Stokes law (Beckman Coulter Allegra 64R, F0850 rotor, centrifugation at 26 900 g for 61 min). Aliquots of supernatant solution were collected and analyzed for metal concentrations by ICP-MS (Perkin-Elmer SCIEX ICP-Mass Spectrometer ELAN DRC II, after sample acidification with TraceSelect grade HNO_3 (2% v/v)), and DIC concentrations on a Shimadzu TOC-V_{CSH}. Each experiment included experimental standards (in duplicate), in which the standards had the same volume of U(VI) stock solution added to a vial in the absence of the clay with pH adjusted to 2.0. In addition, electrolyte blanks (in duplicate) containing 0.1 mol·L^{-1} NaCl but no U(VI) or clay were used to determine calcium and uranium-238 background concentrations (see Electronic Annex).

The U(VI) adsorption results are reported as distribution coefficients (K_D values, in L·kg^{-1}) and fractions of U(VI) adsorbed ($f_{U(VI)_{ads}}$ in %). Adsorbed U(VI) fractions and K_D values were computed based on concentration differences in supernatant solutions between experimental standards (C_{tot}) and samples (C_{eq}):

$$f_{U(VI)_{ads}} = \frac{C_{tot} - C_{eq}}{C_{tot}} \times 100 = \frac{C_{ads}}{C_{tot}} \times 100 \quad (1)$$

$$K_D = \frac{C_{ads}}{m_s \cdot C_{eq}} \quad (2)$$

where m_s is the solid concentration in kg·L^{-1}.

The error bands were calculated as follows (Tournassat et al., 2013):

$$uC_{ads} = \sqrt{uC_{tot}^2 + uC_{eq}^2}; \quad \Delta C_{ads} = k \times uC_{ads} \quad (3)$$

$$uf_{U(VI)_{ads}} = 100 \cdot \sqrt{\left(\frac{uC_{eq}}{C_{tot}}\right)^2 + \left(\frac{C_{eq} \cdot uC_{tot}}{C_{tot}^2}\right)^2};$$

$$\Delta f_{U(VI)_{ads}} = k \times uf_{U(VI)_{ads}} \quad (4)$$

$$uK_D = \sqrt{\left(\frac{uC_{tot}}{m_s \cdot C_{eq}}\right)^2 + \left(\frac{C_{tot} \cdot uC_{eq}}{m_s \cdot C_{eq}^2}\right)^2}; \quad \Delta K_D = k \times K_D \quad (5)$$

where Δ values are the considered error bands, k is the coverage factor (taken at a value of k = 2), C_{tot}, C_{eq}, uC_{tot} and uC_{eq} are the total concentration, the equilibrium concentration and their associated uncertainties (we considered 2 % of the values) respectively. Uncertainty on m_s was neglected.

2.3. Analytical detection limits and background values for dissolved inorganic carbon

The Method Detection Limit (MDL) and Minimum Level (ML) were determined to be 0.051 and 0.161 mg·L^{-1} DIC ($4.2 \cdot 10^{-6}$ and $1.3 \cdot 10^{-5}$ mol·L^{-1} DIC) for the specific setup of our DIC analysis, as described in detail in the Electronic Annex. The MDL represents the minimum DIC concentration that can be identified, measured and reported with a 99 % confidence that the concentration is greater than zero (U.S. EPA, 1995). The ML is defined as the smallest measured concentration of a constituent that may be reliably reported using a given analytical method. Potential DIC contributions from various sources in the CO_2-"free" batch adsorption experiment, performed in the 94.3 % N_2/5.7 % H_2 glove box environment, were quantified as described in detail in the Electronic Annex. Taking into account the offset due to DIC background concentrations in Milli-Q water (MQW), calibration curves showed linearity down to the lowest concentration standard at 0.025 mg·L^{-1} ($2.1 \cdot 10^{-6}$ mol·L^{-1}) of added DIC.

3. EXPERIMENTAL RESULTS

3.1. Dissolved inorganic carbon in experimental solutions

Because U(VI) aqueous speciation is strongly dependent on the DIC concentration (Davis et al. (2004), Fox et al. (2006), and see Figs. EA-1 and EA-2), it was very important in these experiments to determine DIC directly rather than

calculate its concentration based on an assumed equilibrium with a gas phase.

3.1.1. Detection limits and background contributions

DIC background concentrations were similar for MQW before (0.121 $mg \cdot L^{-1}$, $1.0 \cdot 10^{-5}$ $mol \cdot L^{-1}$) and after (0.125 $mg \cdot L^{-1}$, $1.0 \cdot 10^{-5}$ $mol \cdot L^{-1}$) purging with nitrogen gas. The handling of open sample vials in the glove box atmosphere (5 % H_2/95 % N_2) in the CO_2-"free" adsorption experiment, centrifugation of close vials under atmospheric CO_2 conditions, and refrigeration of closed vials outside the glove box prior to DIC analysis were each evaluated for their potential to increase measured DIC concentrations (see Electronic Annex for details). Sample handling and centrifugation, which took place prior to supernatant sampling in the CO_2-"free" adsorption experiment, resulted in 0.344 and 0.277 $mg \cdot L^{-1}$ DIC ($2.9 \cdot 10^{-5}$ and $2.3 \cdot 10^{-5}$ $mol \cdot L^{-1}$ DIC) concentrations during the test experiment. Storage of solutions in the refrigerator, which occurred after supernatant sampling in the adsorption experiments, resulted in a concentration of 0.331 $mg \cdot L^{-1}$ DIC ($2.8 \cdot 10^{-5}$ $mol \cdot L^{-1}$ DIC). Given the similarity of DIC contributions from these potential sources and the series of steps in the CO_2-"free" adsorption experiment, it can be assumed that these DIC concentrations are representative of typical DIC "contaminant" contributions to sample suspensions in our adsorption experiments. Furthermore, we can assume that measured DIC values represent DIC concentrations that were present in sample suspensions during the U(VI) sorption equilibration.

3.1.2. Measured DIC concentrations in batch adsorption experiments

Final dissolved carbonate (DIC) concentrations in the U(VI) sorption experiments were the result of several contributions: (1) background concentrations from reagents (e.g., NaOH), (2) addition of $NaHCO_3$ during initial solution preparation, and (3) ingassing and outgassing of CO_2 during exposure to various gas phases during the preparation of solutions for the U(VI) sorption experiments. A summary of measured DIC concentrations in the adsorption experiments is provided in Fig. 1.

Experiments carried out in the presence of laboratory air (Experiments 1–4) resulted in measured DIC concentrations generally greater than the values expected for this pCO_2 ($\sim 10^{-3.45}$ atm) (Fig. 1, left panel). This was likely due to additions of DIC with reagents, especially during the adjustments of pH with NaOH. Samples from the CO_2-"free" experiment (Experiment 5) had DIC concentrations similar to solutions observed under atmospheric conditions for $pH < 6$, suggesting CO_2 contamination during the experimental handling as described above. However, the samples at $pH > 6$ had DIC concentrations that were much lower than those under atmospheric conditions (Fig. 1, left panel), demonstrating that the contaminant CO_2 ingassing to the solutions was likely flux-limited at higher pH.

In the experiments with elevated CO_2 in the gas phase, the DIC results (Fig. 1, right panel) suggest that neither the gas bag (Experiment 6) or gas chamber (Experiment 7) was sufficiently purged with the 2 % CO_2/98 % N_2 gas to achieve the intended equilibration with the 2% partial pressure of CO_2. This was the case despite multiple purge volumes that were used to clear the bag and gas chamber in these experiments. In experiment 6, solutions up to a pH of 7.24 exhibited DIC concentrations that suggested equilibration with a gas phase composition closer to ~1 % CO_2. Samples from supernatants at higher pH values had DIC concentrations consistent with even lower partial pressures of CO_2. This trend is most likely due to insufficient purging combined with a lack of fast CO_2 equilibration between the aqueous phase and the local atmosphere in the gas bag.

In experiment 7, the calculated low pCO_2 values at acidic pH suggest that the Coy gas chamber was not sufficiently flushed to achieve the target CO_2 partial pressure. Although the solutions contained added $NaHCO_3$ such that they would be equilibrated with a 2 % CO_2 gas phase, DIC data indicate that some CO_2 outgassed from solutions into the chamber atmosphere, driven by a pCO_2 value lower than 2 %.

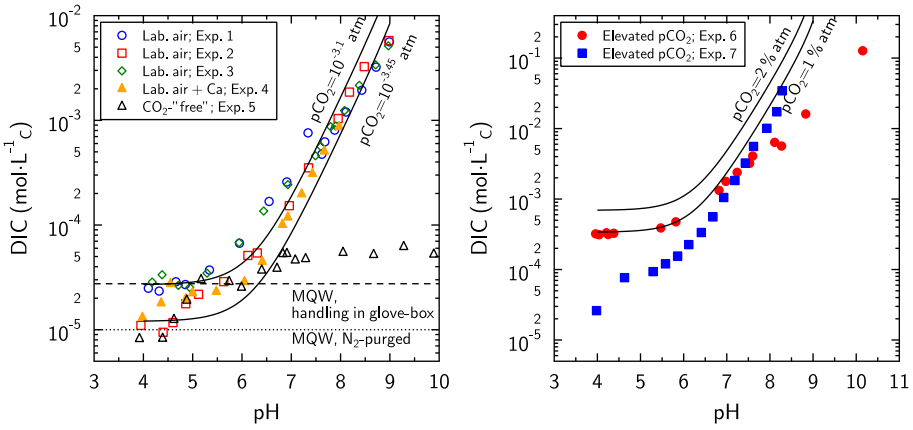

Fig. 1. Measured DIC concentrations as a function of pH in the U(VI) sorption experiments and comparison with values computed for various partial pressures of CO_2. The calculations of DIC concentrations at given pCO_2 partial pressures were carried out using PHREEQC v.3 (Parkhurst and Appelo, 1999, 2013) with the THERMOCHIMIE database (Giffaut et al., 2014).

Despite the problems equilibrating the solutions with the intended gas phases, DIC concentrations in the prepared solutions were constant in the U(VI) sorption experiments after the closing of the centrifuge tubes (calculated partial pressures of CO_2 in the centrifuge tubes are given in Fig. EA-6). By measuring DIC in all sample solutions, including those exposed to laboratory air, the equilibrium geochemical model determined the U(VI) aqueous speciation for each experimental data point rather than assuming a constant specific partial pressure of CO_2 in equilibrium with the aqueous phase. As will be discussed further below, this was very important in describing the observed U(VI) adsorption behavior in the SCM.

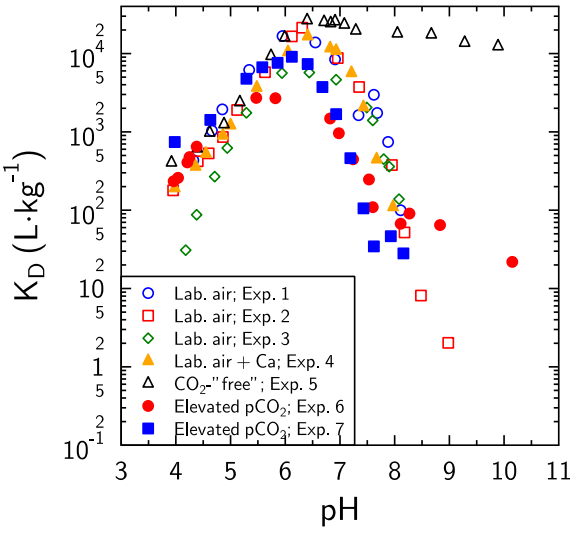

Fig. 2. U(VI) adsorption as a function of pH under variable total U(VI), dissolved inorganic carbon (DIC), and Ca concentrations.

3.2. U(VI) adsorption behavior under varying chemical conditions

3.2.1. Effect of variable DIC

In experiments conducted in laboratory air (Experiments 1–4), U(VI)-montmorillonite K_D values varied over four orders of magnitude as a function of pH (Fig. 2). At low pH, U(VI) adsorption is assumed to be limited due to its competition with protons at surface complexation sites (Stumm et al., 1992). At high pH, low uranium adsorption is attributed to increasing carbonate concentrations, leading to weakly sorbing or non-sorbing aqueous U(VI)-carbonate complexes (Hsi and Langmuir, 1985; Waite et al., 1994; Davis et al., 2004). In the CO_2-"free" system, U(VI) adsorption is very similar at weakly acidic pH values to that observed for the laboratory air atmospheric CO_2 systems. Above pH 6.5, however, U(VI) adsorption was much stronger at very low concentrations of CO_2 than in the laboratory air systems. The increase in U(VI) adsorption at high pH under these conditions can be attributed to much lower concentrations of aqueous U(VI)-carbonate complexes that compete effectively with the edge site surface complexation reactions. The effect of aqueous carbonate complexes on U(VI) adsorption is further demonstrated by the U(VI) adsorption results in systems with elevated CO_2 concentrations (Experiments 6 and 7), where U(VI) adsorption decreased at pH values above 5.5 (Fig. 2).

3.2.2. Effect of variable calcium concentrations

Under laboratory air conditions, U(VI) adsorption appeared to be similar in the presence of 2.1 mmol·L^{-1} $CaCl_2$ compared to Ca background concentrations (Fig. 2). However, upon closer inspection, the U(VI) K_D value appeared to be lower at pH ~ 8 by approximately a half an order of magnitude (compare Exp. 2 and 4 with similar total U(VI) concentrations). Nonetheless, it is difficult

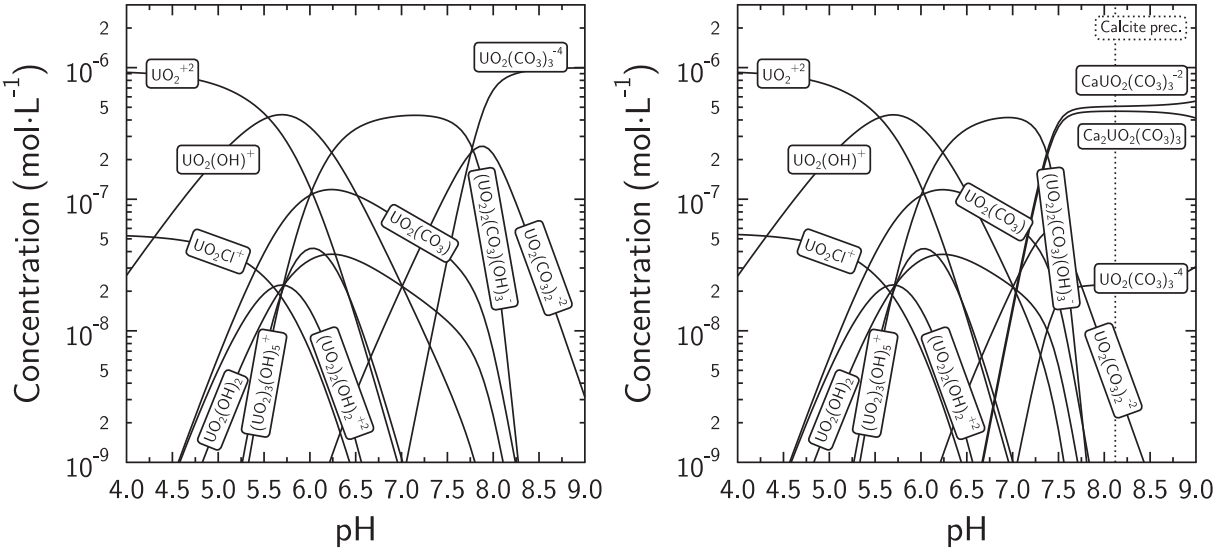

Fig. 3. Calculated aqueous speciation of a 1 micromolar U(VI) solution in 0.1 M NaCl in equilibrium with atmospheric CO_2 (log $pCO_2 = -3.45$) in the absence (left) and presence of 2 mmol·L^{-1} Ca (right). Vertical axis is the negative log of the concentration of each U(VI) species.

to be certain of this effect because of differences in experimentally observed DIC concentrations. Calculations show that U(VI) aqueous speciation changes in this pH region in the presence of sufficient Ca because of the formation of aqueous ternary Ca-U(VI)-carbonate complexes at pH > 7.5 (Fig. 3). This effect is evaluated further in the modeling section, where calculations are made at a constant CO_2 partial pressure.

4. MODELING AND DISCUSSION

4.1. Surface complexation modeling strategy

An analysis of the literature shows that considerable uncertainty remains on the nature of inner-sphere complexes on montmorillonite edge surfaces. Surface complexation modeling cannot elucidate the nature of clay atoms present on surface sites, i.e. decipher the contributions of aluminol, silanol and Fe-substituted sites. However, modeling allows for an estimation of the likelihood of a reaction, such as the adsorption of uranyl carbonate complexes, and an understanding of the effect of Ca-CO_3-U(VI) solution complexes on the extent of U(VI) adsorption in calcium-rich environments. In the process, it is necessary to follow a parsimony rule, i.e. to build a model with the fewest adjustable parameters as possible in order to avoid correlations between fitting parameters. Accordingly, the chosen modeling strategy was based on a four-step approach, as follows. In a first step, U(VI) adsorption model parameters were fitted using experimental data from the CO_2-"free" experiment. In a second step, we applied these parameters to predict the data obtained in the other experiments: a good match of the prediction with experimental data would suggest that formation of ternary uranyl-carbonato surface complexes is not important, while an underestimation of the adsorption extent would indicate that a uranyl-carbonato surface complex must have formed (e.g., see the modeling approach of Waite et al. (1994)). In a third step, we applied the model to a large range of data obtained from the literature in order to test its robustness. In a fourth and final step, factors influencing U(VI) adsorption, such as pCO_2 or Ca^{2+} concentrations, are discussed on the basis of predictive calculations with the model. A summary of experimental U(VI) batch sorption data is provided in the Electronic Annex in order to allow other researchers to test their modeling concepts.

4.2. Surface complexation model for montmorillonite edge surfaces

The objective of the modeling work presented here was to develop a model that was as mechanistic as possible, but without adding too many fitting parameters. Accordingly, the speciation model for SWy-2 edge surfaces was directly taken from Tournassat et al. (2016a). This surface complexation model explicitly takes into account the spillover effect of the basal surface potential on the edge surface potential. This effect is typical for layered minerals with structural charges and renders classical surface complexation models developed for oxide surfaces incorrect for modeling clay mineral edge surface properties (Bourg et al., 2007; Tournassat et al., 2013, 2015a, 2016a).

Briefly, the negative surface charge created by the isomorphic substitutions in the montmorillonite lattice creates a negative electrostatic potential field that interacts with the electrostatic field created by the amphoteric edge surface sites (Secor and Radke, 1985; Chang and Sposito, 1994, 1996). Consequently, if the edge surface charge is zero, the edge surface potential remains negative. This effect can be adequately captured by setting the relationship between surface charge (Q_{edge} in $C{\cdot}m^{-2}$) and surface potential (ψ_{edge} in V) to:

$$\frac{F\psi_{edge}}{RT} = A_1 \ \mathrm{asinh}(A_2(Q_{edge} + A_3)) \tag{6}$$

where A_1, A_2, and A_3 are fitted parameters, F is the Faraday constant (96 485 C mol^{-1}), R is the gas constant (8.314 $J{\cdot}K^{-1}{\cdot}mol^{-1}$) and T is the temperature (K). For montmorillonite at 25 °C, Tournassat et al. (2013) refined the values of these parameters to: $A_1 = 1.4$–$1.2 \log I$, $A_2 = 11 + \log I$, and $A_3 = -0.02 \times (-\log I)^{1.60}$, where I refers to the ionic strength (unitless). This equation is comparable to the classic equation of the diffuse layer model (DLM) for oxides (Davis et al., 1978) that is implemented in most geochemical calculation codes (Steefel et al., 2015), but that is not adapted to model the properties of clay edge surfaces (Tournassat et al., 2013, 2015a, 2016a):

$$\frac{F\psi}{RT} = 2 \ \mathrm{asinh}\ (B \cdot \sigma) \quad \text{with} \quad B = \frac{1}{\sqrt{8\varepsilon\varepsilon_0 RT \cdot 1000 \cdot I}} \tag{7}$$

where $\varepsilon\varepsilon_0$ is the dielectric constant for water. The site densities, stoichiometries and protonation/deprotonation constants were taken from Tournassat et al. (2016a). Site densities were calculated from crystallographic considerations and structural formulas; protonation/deprotonation constants were obtained from the predictions of first-principle molecular dynamics calculations (Liu et al., 2013, 2014, 2015a,b).

Edge surfaces with different crystallographic orientations exhibit amphoteric sites of different natures and with different site densities (Tournassat et al., 2016a). Two kinds of edge surfaces can be found in this model, corresponding to the AC and B chains that were first described by White and Zelazny (1988). The relative proportions of these two kinds of surfaces (AC and B) on SWy-2 particle edges and the total edge specific surface area ($\sim 14\ m^2{\cdot}g^{-1}$) were fitted from titration curves. The value of the edge specific surface area that was fitted by Tournassat et al. (2016a) compared well with the value measured by the low-pressure gas adsorption method ($\sim 19\ m^2{\cdot}g^{-1}$) (Duc et al., 2005). This value, however, was different from the SWy-2 N_2-BET specific surface area value. N_2-BET specific surface area measurements have been commonly used for the calibration of surface complexation models for clay minerals in the literature, even though these values are not representative of the edge specific surface area for the following reason. N_2-BET measurements probe both edge and external basal surface areas of the particles, and the latter contribution always dominates over the first for montmorillonite particles (Tournassat et al., 2003, 2013, 2015a, 2016a,b).

None of the parameters of the above described surface model was changed during the modeling exercises, leaving only the speciation of U(VI) surface complexes and the related association constants as fitting parameters. Only U(VI) surface complexes on the B-chain surface type were considered in the model, in agreement with the results obtained with P-EXAFS on the orientation of the U(VI) surface complexes (Schlegel and Descostes, 2009; Marques Fernandes et al., 2012). In the absence of any supporting spectrometric evidence on the nature of the surface sites involved in U(VI)-specific adsorption, we hypothesized that the formation of U(VI) surface complexes took place on the most abundant, non-substituted Si_T-Al_{Oc}-Si_T edge sites, where subscripts T and Oc refer to the tetrahedral and octahedral sheets of the layer respectively (Table 2). Note that the influence of cation exchange reactions was negligible under our experimental conditions.

An in-house version of PHREEQC, which was modified to handle Eq. (6), was used to carry out the calculations, together with the database THERMOCHIMIE v. 9b0 for thermodynamic parameters of solute species (Giffaut et al., 2014). This database is available in various formats including PHREEQC format at the following address: https://www.thermochimie-tdb.com/.

Table 2
U(VI) surface complexation reactions on SWy-2 particle edges and related association constants used for modeling. The surface speciation model of Tournassat et al. (2016a) provides information on surface types and areas, site types and protonation/deprotonation constants. For the calculation of the sites stoichiometry, the following structural formula was considered: $(Si_{3.87}Al_{0.13})(Al_{1.52}Mg_{0.25}Fe^{III}_{0.224}Fe^{II}_{0.006})Na_{0.36}O_{10}(OH)_2$ (Duc et al., 2005; Tournassat et al., 2016a).

Edge surface areas	Total	$14\ m^2\cdot g^{-1}$
	Edge surface of B type	$7\ m^2\cdot g^{-1}$
Protonation/deprotonation reactions	Log K	
	Si_T-Al_{Oc}-Si_T	Si_T-Fe^{III}_{Oc}-Si_T
$>SiteH_4^+ = >SiteH_3 + H^+$	−3.1	−1.2
$>SiteH_3 = >SiteH_2^- + H^+$	−7	−5.1
$>SiteH_2^- = >SiteH^{2-} + H^+$	−7	−8.6
$>SiteH^{2-} = >Site^{3-} + H^+$	−8.3	−8.6
	Si_T-Mg_{Oc}-Si_T	Si_T-Fe^{II}_{Oc}-Si_T
$>SiteH_4 = >SiteH_3^- + H^+$	−10.8	−6.6
$>SiteH_3^- = >SiteH_2^{-2} + H^+$	−10.8	−10.2
$>SiteH_2^{-2} = >SiteH^{-3} + H^+$	−13.2	−10.2
$>SiteH^{-3} = >Site^{-4} + H^+$	N.A.	−11.2
	Al_T-Al_{Oc}-Si_T	
$>SiteH_4 = >SiteH_3^- + H^+$	−4.9	
$>SiteH_3^- = >SiteH_2^{-2} + H^+$	−7	
$>SiteH_2^{-2} = >SiteH^{-3} + H^+$	−8.5	
$>SiteH^{-3} = >Site^{-4} + H^+$	−15.1	
U(VI) adsorption reactions on Si_T-Al_{Oc}-Si_T sites		Log K
$>SiteH_3 + UO_2^{2+} = >SiteH_3UO_2^{2+}$		4.8
$>SiteH_3 + UO_2^{2+} = >SiteHUO_2 + 2\ H^+$		−4.8
$>SiteH_3 + UO_2^{2+} + 2\ H_2O = >SiteUO_2(OH)_2^{-3} + 5\ H^+$		−25.3

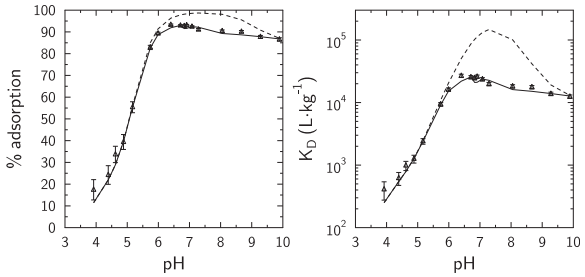

Fig. 4. U(VI) adsorption results in the CO_2-"free" experiment (symbols: data; lines: model predictions) plotted as percentages of U(VI) adsorbed (left) and adsorption distribution coefficients (K_D, right). The reference model (solid line) was calculated taking into account individually measured DIC concentrations for each data point. The dashed line corresponds to a prediction using the same model parameters but while assuming zero DIC concentrations. Solid concentration = 0.52 g·L^{-1}, total U(VI) concentration = $1.1 \cdot 10^{-6}$ mol·L^{-1}, [NaCl] = 0.1 mol·L^{-1}.

4.3. Calibration of the U(VI) surface complexation model in the "absence" of CO_2

Carrying out all the steps of an adsorption experiment in the complete absence of CO_2 is very difficult. The DIC measurements indicate that carbonate was not fully excluded from the solutions despite the efforts to achieve this goal. Despite the observed carbonate contamination, the adsorption results from the CO_2-"free" experiments were qualitatively similar to other literature data for carbonate-free systems (Bradbury and Baeyens, 2005; Marques Fernandes et al., 2012), i.e. showing a sharp increase in U(VI) adsorption from pH 4 to pH 6 and a limited decrease of U(VI) adsorption at pH > 6 (Fig. 2).

While measured DIC concentrations are usually not considered in CO_2-"free" U(VI) adsorption models in the literature, they were specifically taken into account in the model calculations discussed here. Only three edge surface reactions were necessary to reproduce the data (Fig. 4 and Table 2). The effect of cation exchange was negligible because of the effective competition between Na^+ and UO_2^{2+} for cation exchange sites under our experimental conditions (0.1 M NaCl background electrolyte). The calculation made with the same reference model parameters, but using a zero DIC value instead of the measured one, illustrates how sensitive the calculation is to the consideration of actual DIC values (dashed line in Fig. 4) Even at the low DIC concentrations observed in the CO_2-"free" experiment, dissolved carbonates provide highly competitive ligands for U(VI) complexation reactions relative to mineral surface sites.

4.4. Blind prediction of U(VI) adsorption in the presence of CO_2

The minimal set of adsorption parameters obtained from the fitting of CO_2-"free" adsorption data were directly

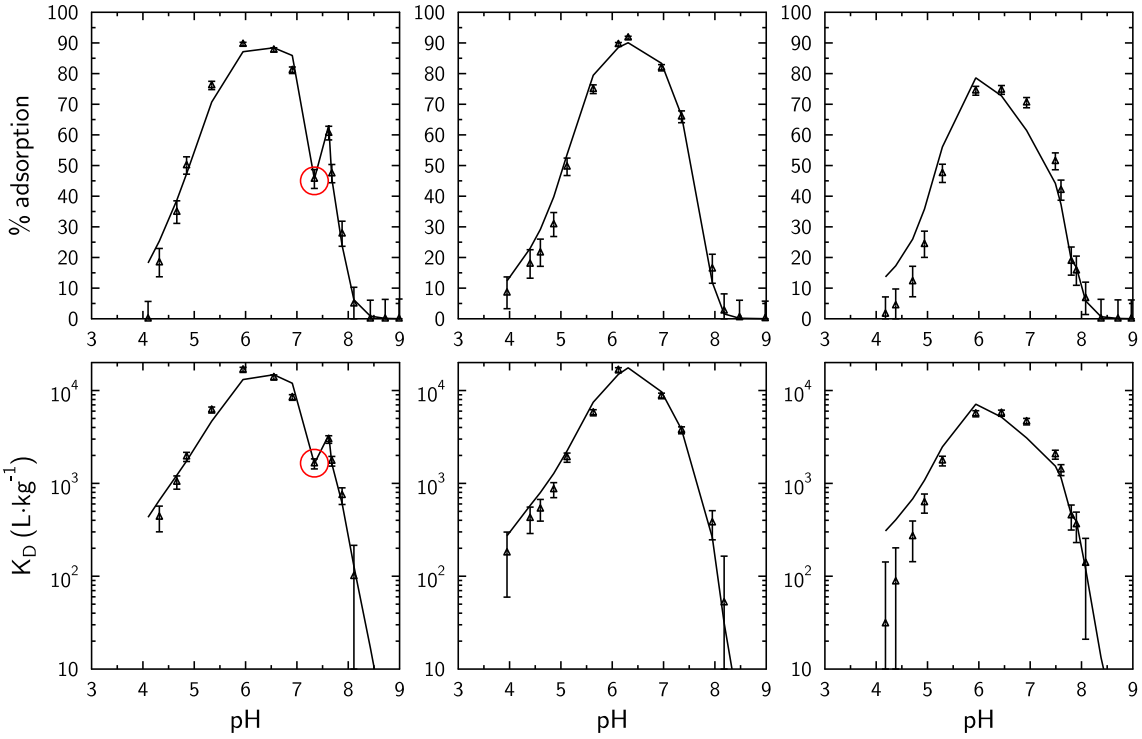

Fig. 5. U(VI) adsorption results in laboratory air in a NaCl background electrolyte concentration of 0.1 M (symbols: data; line: model predictions). The model was calculated for each data point taking into account individually measured DIC concentrations. The solid concentration was ~0.52 g·L^{-1}. From left to right, the total U(VI) concentration was $1.1 \cdot 10^{-7}$, $9.6 \cdot 10^{-7}$, or $2.55 \cdot 10^{-6}$ mol·L^{-1}. $NaHCO_3$ aliquot addition was twice the intended amount for the sample at pH = 7.34 and $1.1 \cdot 10^{-7}$ mol·L^{-1} U(VI) (circled experimental point in left panel).

used to predict the results of experiments carried out under laboratory air conditions (Experiments 1–3). The individually measured DIC concentrations were used to calculate the aqueous composition and U(VI) speciation. The blind prediction of U(VI) adsorption data was good (Fig. 5). Furthermore, in the experiment at $U(VI)_{tot} = 0.1$ μM, the $NaHCO_3$ aliquot addition was twice of what it should have been for the sample at pH = 7.34, due to an experimental error (see point circled in left panel of Fig. 5). The related decrease in U(VI) adsorption due to U(VI) aqueous complexation with carbonate was reproduced by the model, without a need for including the formation of uranyl-carbonato complexes on the montmorillonite surface. This further supports doubts from spectroscopic studies on the existence of such ternary surface complexes (on montmorillonite) at atmospheric pCO_2 conditions. Furthermore, the experimental error in the $NaHCO_3$ addition for the sample at pH 7.34 also demonstrates that the solution was slow to re-equilibrate with the atmosphere outside of the closed sample vial, and confirms that the measured DIC values were constant during U(VI) sorption equilibration.

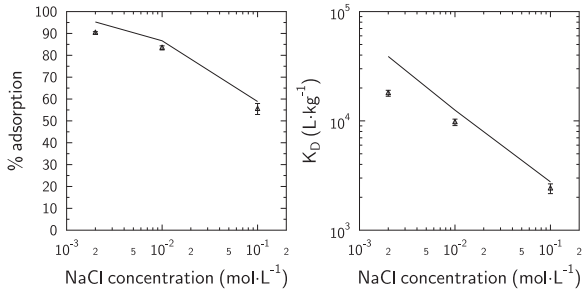

Fig. 6. U(VI) adsorption as a function of ionic strength under laboratory air conditions (symbols: data; line: model predictions). The model prediction was calculated for each data point taking into account individually measured DIC concentrations and pH values (5.6, 5.4, 5.2 at 0.002, 0.01 and 0.1 M NaCl, respectively). The solid concentration was 0.52 g·L^{-1}; the total U(VI) concentration was $9.5 \cdot 10^{-7}$ mol·L^{-1}.

The robustness of the model was further tested as a function of ionic strength, and, again, the model predicted the data well (Fig. 6). Under the conditions of this experimental dataset, the influence of cation exchange reactions was negligible for pH > 5. The apparent effect of ionic strength on the extent of U(VI) adsorption is due to the changes in electrostatic potential as a function of ionic strength, as well as to small changes in pH values (see Fig. 6 caption).

At greater DIC concentrations (due to elevated pCO_2), U(VI) adsorption data were also correctly predicted by the model without changing fitting parameters or adding new surface complexes. The model underpredicted the measured values in percent U(VI) adsorbed by 15% or less (Fig. 7). However, it was not possible to enhance the quality of the fit by including a uranyl-carbonato surface complex without deteriorating the data fits obtained in laboratory air or CO_2-"free" conditions.

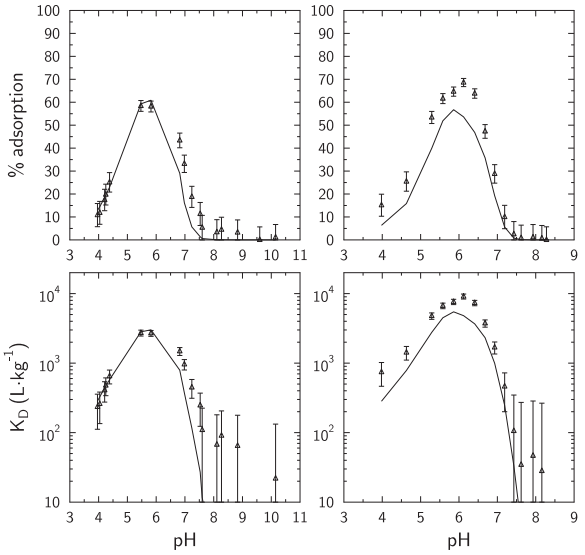

Fig. 7. U(VI) adsorption in the presence of elevated pCO_2 (symbols: data; line: model predictions). The model was calculated for each data point taking into account individually measured DIC concentrations. Solid concentrations were 0.52 g·L^{-1} (left) or 0.24 g·L^{-1} (right). Total concentrations of U(VI) were $8.1 \cdot 10^{-7}$ mol·L^{-1} (left) and $9.8 \cdot 10^{-7}$ mol·L^{-1} (right).

Table 3
Cation exchange reaction parameters added to the reference model in order to reproduce literature data obtained at low ionic strength and low pH.[a]

Surface reactions on montmorillonite basal surfaces	Log_{10} K	
$X^- + Na^+ = XNa$	0	
Cation exchange reactions with U(VI) species (as a function of literature data)	Log_{10} K	CEC (mol·kg^{-1})[b]
Troyer et al. (2016), Hyun et al. (2001)		
$2\ XNa + UO_2^{2+} = X_2\ UO_2 + 2\ Na^+$	0.95	0.9
Pabalan et al. (1996)		
$2\ XNa + UO_2^{2+} = X_2\ UO_2 + 2\ Na^+$	0.75	1.2
McKinley et al. (1995)		
$2\ XNa + UO_2^{2+} = X_2\ UO_2 + 2\ Na^+$	1.2	0.8
Turner et al. (1996)		
$2\ XNa + UO_2^{2+} = X_2\ UO_2 + 2\ Na^+$	0.7	0.41

[a] Cation exchange reactions were modeled with a classic diffuse layer model that was already calibrated for Na^+ and Ca^{2+} by Tinnacher et al. (2016). The total specific surface area for cation exchange reactions was set to the crystallographic surface area for montmorillonite, i.e. ~750 m^2·g^{-1} (Tournassat and Appelo, 2011; Tournassat et al., 2011, 2015b; Tournassat and Steefel, 2015).
[b] Values measured in the reference papers.

4.5. Model predictions of literature data

A wide range of literature data is available for U(VI) adsorption on montmorillonite (McKinley et al., 1995; Pabalan and Turner, 1996; Turner et al., 1996; Hyun et al., 2001; Bradbury and Baeyens, 2005; Marques Fernandes et al., 2015; Troyer et al., 2016). Thus, it was possible to test the predictive capabilities of the model over a wider range of conditions than those tested in the experiments described above. However, the limitations of this benchmarking approach are at least twofold. First, the origin and preparation of the clay material (fine fraction separation and further chemical purification) can influence adsorption results because of variations in reactive surface area and surface chemistry. Second, DIC concentrations were not reported in previous studies, while the results presented here demonstrate the importance of this parameter.

The following modeling and data presentation strategies were applied in order to avoid any misinterpretations regarding the quality of the model predictions. Data from the literature were first compared with a blind modeling prediction without any adjustment of model parameters given in Table 2 (reference model). In the case of experiments carried out under atmospheric conditions, a $log_{10}(pCO_2)$ value of −3.45 was assumed for these reference calculations. In case of CO_2-"free" conditions, a $log_{10}(pCO_2)$ value of −99 was applied. In a second step, various hypotheses were tested to achieve a better fit of the data, if necessary. In particular, as our reference model did not include cation exchange reactions, it was necessary to include these reactions to reproduce U(VI) adsorption

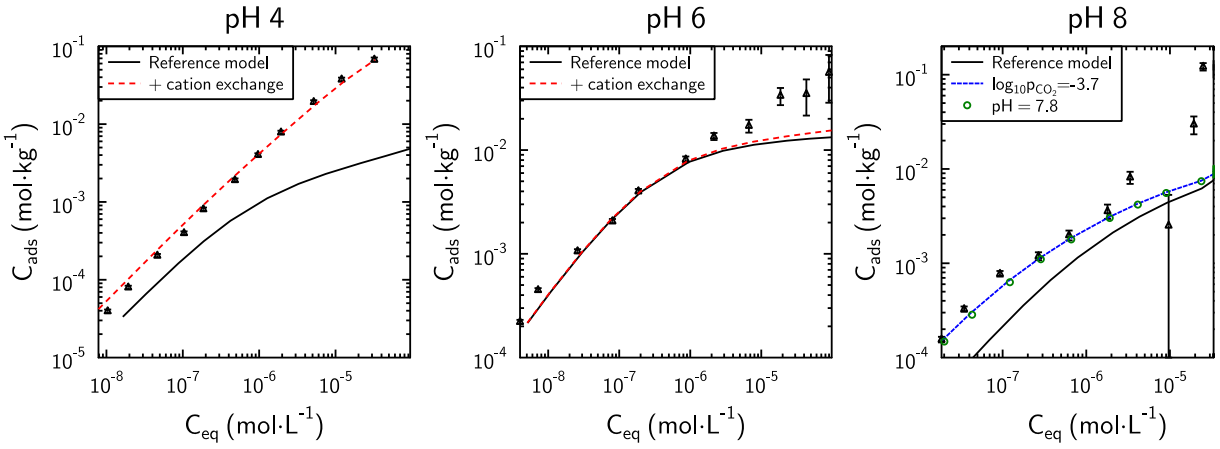

Fig. 8. Comparison of model predictions with the U(VI) adsorption data on montmorillonite of Troyer et al. (2016).

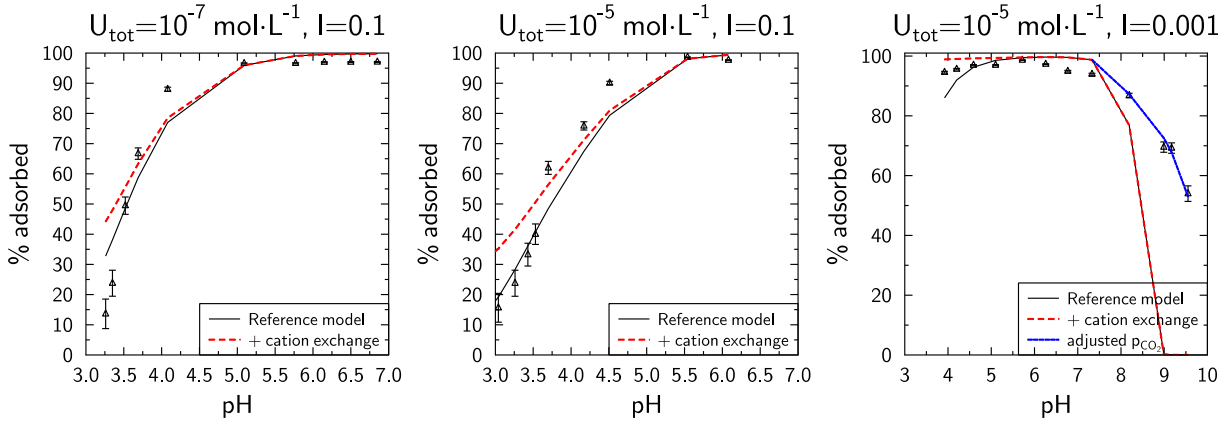

Fig. 9. Comparison of model predictions with the U(VI) adsorption data on montmorillonite of Hyun et al. (2001).

data obtained at low ionic strength and low pH (pH < 4) conditions.

4.5.1. Data of Troyer et al. (2016)

The data of Troyer et al. (2016) were acquired in the presence of atmospheric pCO_2 on a clay material similar to the one used in this study (<2 µm fraction of SWy-2 montmorillonite), but in the presence of a 0.01 M NaCl electrolyte, thus promoting cation exchange reactions compared to our conditions. We tested the model on the authors' three adsorption isotherms obtained at pH 4, 6 and 8. Data obtained at pH 6 could be adequately reproduced without changing any parameter from the reference model (Fig. 8). Data obtained at pH 4 could be reproduced only by adding a cation exchange reaction to the reference model (Table 3). Data at pH 8 were not satisfactorily reproduced in the first calculations. However, a slight change in the pH value (7.8 instead of 8) or pCO_2 value ($10^{-3.7}$ atm instead of $10^{-3.45}$ atm) made it possible to fit the data very well, again showing the great sensitivity of the system to pH/pCO_2 over this range of conditions.

Some data at high U(VI) surface coverage could not be predicted by the model, even after changing some of the parameters. The origin of this problem can be understood by comparing the measured U(VI) surface coverage with the maximum available surface site density. If we consider a site density of 2.06 sites·nm^{-2} (Bourg et al., 2007; Tournassat et al., 2016a) and a specific surface area of 14 m^2·g^{-1}, the maximum adsorption capacity for U(VI) complexes should be ~0.05 mol·kg^{-1}. If we further assume that no U multinuclear complexes form at the surface, this value decreases to ~0.025 mol·kg^{-1} (perfect ordering). This value is similar to the maximum adsorbed concentration value measured in Troyer et al. (2016) at pH 6, but far lower than the maximum value measured at pH 8. Hence, the much higher measured than simulated extent of U(VI) adsorption cannot be explained by the formation of isolated mononuclear bidentate U(VI) surface complexes alone. These data must include additional uptake processes that are not described in the model developed here, and are beyond the scope of this study, e.g. polymerization on the surface, or precipitation. The latter cannot be fully ruled out at elevated U(VI) concentrations, since a supersaturation of schoepite was predicted at 1.3 and 62 µmol·L^{-1} U(VI) at pH 6 and pH 8 respectively, based on the U(VI) aqueous speciation model of Troyer et al. (2016).

4.5.2. Data of Hyun et al. (2001)

The data of Hyun et al. (2001) were also acquired in the presence of atmospheric pCO_2 on a clay material similar to the one used in this study (fine fraction of SWy-2 montmorillonite). U(VI) adsorption was characterized at two fixed total U(VI) concentrations (10^{-7} and 10^{-5} mol·L^{-1}), with variable pH, and for two ionic strengths (I = 0.001 and I = 0.1), and at a relatively high solid concentration (~6–7 g·L^{-1}). The reference model provided a good prediction of the data (Fig. 9).

At low ionic strength, the addition of cation exchange reactions, with the same parameters as for the study of Troyer et al. (2016), had almost no influence on the results. At pH 4 and low ionic strength, the high level of adsorption is mainly due to the increase in the surface potential value at edge surfaces. At high pH, the disagreement between experimental data and model predictions could be attributed to the fact that carbonate concentrations were not constrained experimentally (Hyun et al., 2001). Pabalan and Turner (1996) reported that, under some conditions, an equilibration period of ten days with the atmosphere was necessary to reach equilibrium between DIC and

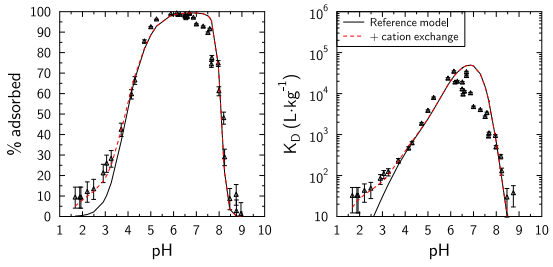

Fig. 10. Comparison of model predictions with U(VI) adsorption data of Pabalan and Turner (1996). Cation exchange parameters are given in Table 3. Solid concentration = 3.2 g·L^{-1}; total U(VI) concentration = $2 \cdot 10^{-7}$ mol·L^{-1}. The results are presented in percentage adsorbed (left) and in $\log_{10}$ K_D values (right) for a better evaluation of model fits at low (left) and high (right) U(VI) adsorption.

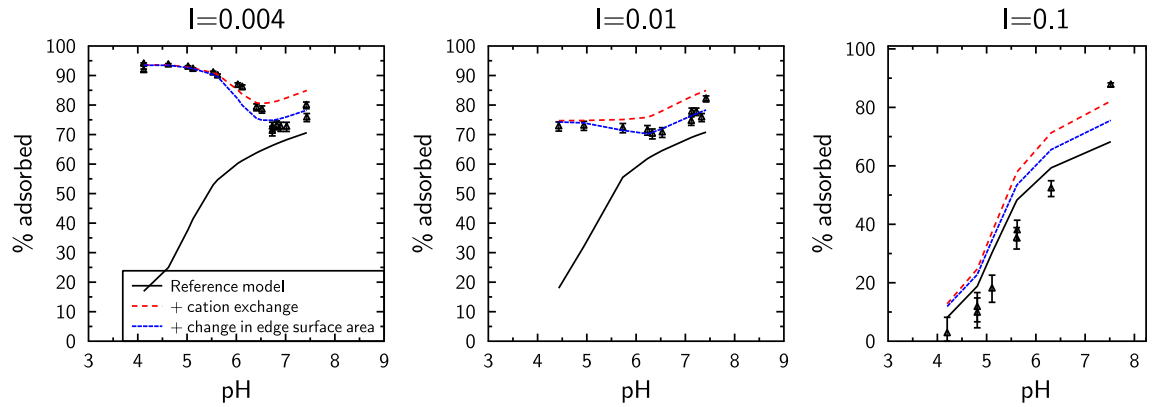

Fig. 11. Comparison of model predictions with U(VI) adsorption data of McKinley et al. (1995). For the blue curve, the total edge specific surface area was set to 12.6 $m^2 \cdot g^{-1}$ instead of the reference model value of 14 $m^2 \cdot g^{-1}$. Cation exchange parameters are given in Table 3.

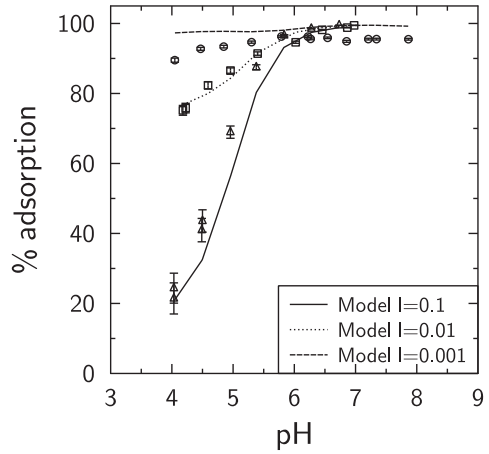

Fig. 12. Comparison of model predictions (lines) with U(VI) adsorption data of Turner et al. (1996) (symbols). Cation exchange parameters are given in Table 3.

atmospheric CO_2. Insufficient time of equilibration with the atmosphere in the experiments of Hyun et al. (2001) could have led to pCO_2 values that were lower than the atmospheric value considered in the calculations: fitted value were $\log_{10}$ $pCO_2 = -4.4$ at pH 9 and -5.05 at pH 9.55 (blue[1] line in Fig. 9).

4.5.3. Data of Pabalan and Turner (1996)

The data of Pabalan and Turner (1996) were obtained in the presence of atmospheric pCO_2 on a clay material, SAz-1, that was different from SWy-2. Experimental conditions were otherwise quite similar to those used in the present study. In particular, close equilibrium with atmospheric pCO_2 was ensured by the addition of bicarbonate to the solutions. Again, the predictions of the model were in very good agreement with the experimental data without any further adjustments (Fig.10), despite the different nature of the clay.

[1] For interpretation of color in Fig. 9, the reader is referred to the web version of this article.

4.5.4. Data of McKinley et al. (1995)

McKinley et al. (1995) reported U(VI) adsorption data on the <2 μm fraction of Swy-1 montmorillonite as a function of pH and ionic strength. At first sight, these data were not satisfactorily reproduced by the reference model (Fig. 11). The addition of cation exchange reactions improved predictions at low pH, but U(VI) adsorption at pH > 5.5 was still overestimated. However, these discrepancies can be satisfactorily explained by taking into account that the edge specific surface area of the Swy-1 sample from McKinley et al. (1995) was lower than the area of the Swy-2 sample, i.e. 12.6 $m^2 \cdot g^{-1}$ instead of 14 $m^2 \cdot g^{-1}$. Both values are within the range of montmorillonite edge surface area values reported in the literature, which vary from 5 $m^2 \cdot g^{-1}$ to 25 $m^2 \cdot g^{-1}$ (Tournassat et al., 2015a, 2016a).

4.5.5. Data of Turner et al. (1996)

Turner et al. (1996) reported U(VI) adsorption data on the <2 μm fraction of a smectite isolate from a sedimentary rock fraction (Kenoma scmectite). Kenoma smectite is a beidellite, meaning that most of its structural charge originates from tetrahedral isomorphic substitutions, instead of octahedral substitutions for montmorillonite. Despite this difference, U(VI) adsorption data could be fitted equally well using the same approach as for the data of McKinley et al. (1995). Only U(VI) adsorption data obtained at very low ionic strength ($I = 0.001$) were overestimated (Fig. 12). Since the solid/liquid separation was achieved by centrifugation, it may be possible that finer particles were not completely removed from solution at this ionic strength, causing a lower apparent extent of U(VI) adsorption. (At low ionic strength, separation of solids from solution based on density differences is more difficult, due to the increased intensity of electrostatic repulsive interactions between montmorillonite layers (Van Olphen, 1992)).

4.5.6. Data of Marques Fernandes et al. (2012)

Marques Fernandes et al. (2012) conducted U(VI) adsorption experiments on the <0.5 μm fraction of a SWy-1 montmorillonite over a wide range of pH and total U(VI) concentrations while varying pCO_2. Experimental data at pH > 7, in the presence and absence of atmospheric

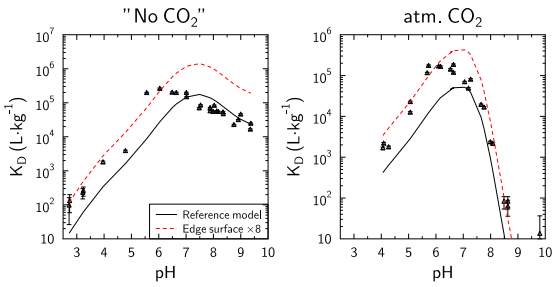

Fig. 13. Comparison of model predictions (lines) with experimental U(VI) adsorption data on montmorillonite of Marques Fernandes et al. (2012) (symbols).

pCO_2 (actual DIC concentrations were not measured), were predicted satisfactorily by the reference model without further modifications (Fig. 13). Experimental data obtained at lower pH, however, had higher adsorption than predicted by the reference model. The position of the pH adsorption edge could only be reproduced by increasing the edge surface area by a factor 8. This is probably not a justifiable assumption, even if we consider that the authors used a finer clay fraction (<0.5 μm) than in most other reported studies (<2 μm). With the large edge surface area, U(VI) adsorption was also greatly overestimated at pH > 7 (Fig. 13). The SWy-1 montmorillonite material of Marques Fernandes et al. (2012) thus exhibits U(VI) adsorption properties that are significantly different from the SWy-1 material studied by McKinley et al. (1995) and all other montmorillonite materials studied in the literature, given the otherwise good agreement between experimental data and the model predictions presented here for a large number of other studies. Based on the quality of fit, Marques Fernandes et al. (2012) attributed the very high adsorption affinity of SWy-1 montmorillonite to "strong sites", with a specific site density of ~2 mmol·kg^{-1}. However, if present, the influence of such strong sites should have been apparent in the many other studies discussed above, where the U(VI) to solid concentration ratio was lower than the putative "strong site" density. Hence, it appears that, for most other solid materials previously studied, these strong sites either do not exist or are present at a far lower site density than the reported value of ~2 mmol·kg^{-1} (Marques Fernandes et al. (2012)). Differences in material preparation procedures could potentially explain this difference in reactivity; e.g., Marques Fernandes et al. (2012) acidified their clay sample to pH 3.5 to remove acid-soluble impurities, while pH 5 was used in this and other previous studies.

Marques Fernandes et al. (2012) also conducted U(VI) adsorption experiments in the presence of added $NaHCO_3$ in order to probe the adsorption of U(VI)-carbonate complexes at the surface. These data could be predicted with our model after an adjustment of the equilibrium DIC concentrations (Fig. 14). Our calculations led to the conclusion that the equilibrium DIC value was 30 % to 40 % lower than the initially guessed values. Since measured DIC values are not available from the above reference, it is not possible to give a definitive conclusion with regards to the adequacy of the model prediction with the data. However,

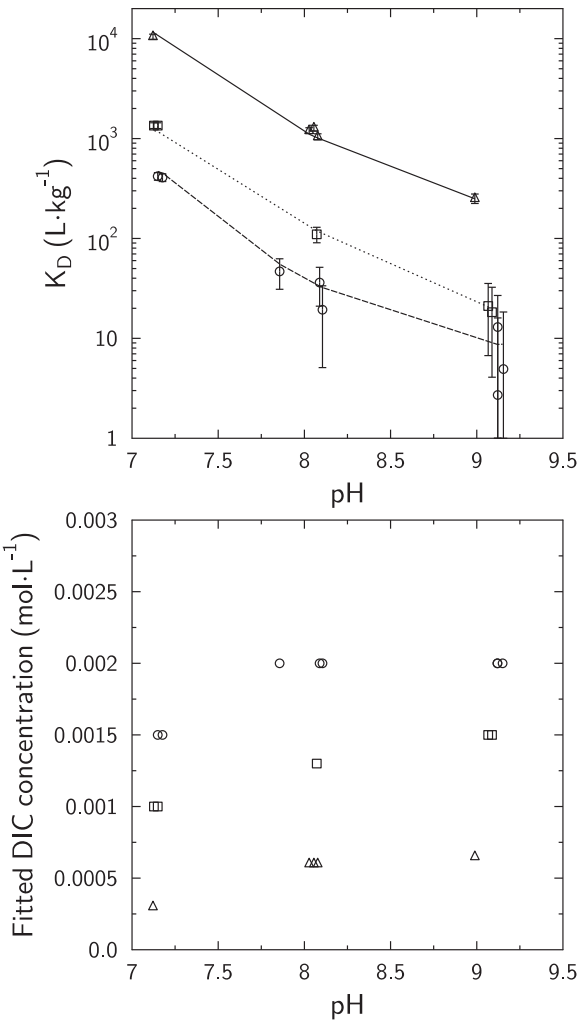

Fig. 14. Top: comparison of model predictions (lines) with experimental U(VI) adsorption data on montmorillonite of Marques Fernandes et al. (2012) in the presence of added $NaHCO_3$ guessed concentration of 1 mmol·L^{-1} (triangles), 3 mmol·L^{-1} (squares), and 5 mmol·L^{-1} (circles). The actual values of DIC were adjusted in order to fit the data. Fitted DIC values are plotted in the bottom figure.

the discrepancy between *guessed* and *fitted* DIC values is similar to the one that we recorded in our own experiments between *guessed* and *measured* values (see materials and methods section and Fig. 2). Hence, we believe that Marques et al. (2012) may have experienced similar, experimental problems.

4.6. Summary of modeling results

The reference U(VI) adsorption model presented here is based on a state-of-the-art description of the reactivity of montmorillonite clay edges that specifically takes into account the spillover effect of the basal surface potential on the edge surface potential (Bourg et al., 2007; Tournassat et al., 2013, 2015a, 2016a). This model accurately predicts adsorption of U(VI) on montmorillonite surfaces over a wide range of experimental conditions, with

only one specific adsorption site, three different U(VI) complexes at the surface, and one cation exchange reaction.

Within the limits of data accuracy, there was no need to include the formation of uranyl-carbonato surface complexes in the model to simulate the experimental data. Including such a species would only be justified if: (1) the discrepancies between experimental data and model predictions (without including these surface complexes) were larger than the combined uncertainties associated with experimental errors and formation constants for aqueous U(VI)-carbonate complexes, and (2) if actual measurement data are available for all solution parameters, including DIC concentrations (or alternatively, alkalinity). Without these data, the uncertainties of assumed pCO_2 values are too large to draw any conclusions regarding the presence of ternary U(VI)-carbonato surface complexes.

For illustration, the effect of varying pCO_2 conditions on U(VI) adsorption is shown in Fig. 15. Based on these calculations with the reference model, at pH > 9 a "true" absence of CO_2 can be interpreted only if it can be demonstrated that actual pCO_2 values are lower than 10^{-6} atm. This partial pressure corresponds to 1 ppm CO_2 in the surrounding atmosphere, i.e. experimental conditions that could be met only with great difficulty in the laboratory, even in a specially equipped glove box. It can be concluded that an "absence of CO_2" at pH > 9 (ideally corresponding to $pCO_2 = 10^{-99}$ atm in Fig. 15), is, in fact, obtained because of slow gas exchange rates between degassed solutions and the surrounding atmosphere, and not a true equilibrium with the partial pressure of CO_2 in that atmosphere. Under these conditions, it is thus necessary to measure DIC concentrations to assess the exact concentrations in solutions exposed to low levels of pCO_2. To our knowledge, this type of measurement has never been performed in previously reported U(VI) adsorption studies on montmorillonite. Most likely, this has sometimes led to false assumptions that previous experiments were conducted at pCO_2 levels that did not impact U(VI) adsorption.

For example Schlegel and Descostes (2009) reported U(VI) adsorption results in the "absence of CO_2" that clearly show evidence of pCO_2 at higher values than 10^{-5} atm (compare their Fig. 1 with Fig. 15 of this paper). Even a precise interpretation of data obtained at atmospheric pCO_2 may be problematic. The value of atmospheric pCO_2 can fluctuate as a function of geographic location, season, and above all the presence of humans in an enclosed lab setting because of respiration and poor ventilation. In addition, a slight change in pH after pre-equilibration of a solution (e.g., due to reagent addition) can impact the final pCO_2 value in a reaction vessel if the time-frame of the pH re-adjustment is too short to allow for full gas-solution re-equilibration. A pCO_2 of $10^{-3.2}$ instead of $10^{-3.45}$ atm has a significant effect on the prediction of U(VI) adsorption at pH > 7. Hence, even with a 'forced' pre-equilibration of background electrolyte solutions using $NaHCO_3$ additions for intended pH values, CO_2 exchange with the surrounding atmosphere and other experimental artefacts add a significant uncertainty to the modeling results, unless actual measured DIC concentrations are used during the model fitting process. This effect is well illustrated with the modeling of U(VI) adsorption data by Troyer et al. (2016) at pH ~ 8 (Fig. 12).

While DIC concentrations are critical parameters in the evaluation of U(VI) adsorption, the combined presence of Ca and carbonate further increases the level of complexity and uncertainty in the model calculations. This is due to the formation of aqueous calcium-uranyl-carbonate complexes (Meleshyn et al., 2009), with unknown adsorption impacts (Fox et al., 2006). According to the reference model, the effect of the formation of this complex on U(VI) adsorption could be significant for Ca^{2+} concentrations larger than 2 mmol·L^{-1}, which is in agreement with our experimental results (Fig. 16).

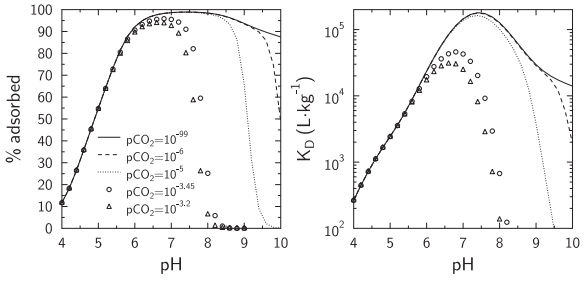

Fig. 15. Predicted effect of pCO_2 on U(VI) adsorption onto montmorillonite using the reference model with a solid concentration of 0.5 g·L^{-1}, a 0.1 M NaCl background electrolyte and a total U(VI) concentration of 10^{-7} M.

5. CONCLUSIONS AND ENVIRONMENTAL IMPLICATIONS

Overall, we can summarize the major findings and implications of this study in the following:

1. We developed a new surface complexation model (SCM) that specifically accounts for the 'spillover' of the electrostatic surface potential of basal cation exchange sites on the surface potential of neighboring edge sites. This model allows us to simulate U(VI) adsorption onto Na-montmorillonite over a wide range of chemical solution conditions with a lower number of fitting parame-

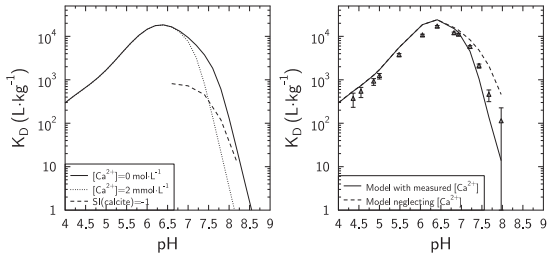

Fig. 16. Left: Predicted effect of Ca^{2+} concentration on U(VI) adsorption using the reference model with a solid concentration of 0.5 g·L^{-1}, a 0.1 mol·L^{-1} NaCl background electrolyte, a total U(VI) concentration of 10^{-6} mol·L^{-1}, and a $pCO_2 = 10^{-3.2}$ atm. Solubility index (SI) for calcite is plotted for comparison. Right: Comparison of our experimental data with model results with and without taking into consideration the impact of Ca^{2+} on U(VI) solution speciation.

ters than previous SCM concepts, and without including a second site type or the formation of ternary U(VI)-carbonato surface complexes. This SCM allows us to simulate U(VI) sorption onto montmorillonite as a function of chemical solution conditions, while minimizing the number of fitting parameters in subsequent uranium(VI) diffusion models.

2. Modeling results suggest that an accurate description of the unique characteristics of electrostatic surface potentials on montmorillonite edge sites is highly important, in order to accurately predict U(VI) sorption and transport behavior at larger field scales. Similar modeling approaches may also be useful for other charge-unbalanced, layered mineral phases.
3. Our modeling results further emphasize the strong influence of dissolved carbonate ligands on U(VI) sorption, which is driven by the competition between U(VI)-carbonate complexation reactions in solution and U(VI) surface complexation reactions on montmorillonite edge sites. As a consequence, predictive U(VI) transport models need to capture potential changes in dissolved inorganic carbon (DIC) concentrations over time and space, e.g. in case of variable contents in carbonate minerals along transport pathways and/or fluctuating pH conditions. For instance, calcite impurities in bentonite, the proposed buffer material at future nuclear waste repositories, may affect U(VI) sorption by providing a source of dissolved carbonate concentrations.
4. Lastly, a measurement of DIC concentrations appears to be crucial for accurate simulations of U(VI) aqueous speciation during the development and calibration of SCMs. Assumptions of a full exclusion of inorganic carbon from sample solutions in CO_2-"free" adsorption experiments, or a complete solution equilibration with atmospheric/elevated CO_2 levels in the local atmosphere, may often not be justified. This is due to the generally challenging nature of CO_2-"free" adsorption experiments, and the potentially slow CO_2 gas exchange between sample solutions and the local atmosphere under atmospheric/elevated CO_2 conditions. Hence, we recommend that DIC analysis or alkalinity titrations are included as routine measurements in future U(VI) adsorption studies. Furthermore, future experimental designs should also take into account the experimental challenges experienced in this study, with regards to achieving constant pCO_2 conditions across a series of sample solutions in a given adsorption experiment.

ACKNOWLEDGEMENTS

J.A.D. acknowledges funding from L'Institut Carnot for his visit to the BRGM. S.G. acknowledges funding by the French National Research Agency (ANR, grant ANR-14-CE01-0006). This research was supported in part by the U.S. Department of Energy under Contract DE-AC02-05CH11231 under the auspices of the Used Fuel Disposition program (Office of Nuclear Energy).

APPENDIX A. SUPPLEMENTARY MATERIAL

Supplementary data associated with this article can be found, in the online version, at https://doi.org/10.1016/j.gca.2017.09.049.

REFERENCES

Adinarayana K. N. V., Sasidhar P. and Balasubramaniyan V. (2013) Modelling of calcium leaching and its influence on radionuclide migration across the concrete engineered barrier in a NSDF. *J. Environ. Radioact.* **124**, 93–100.

Arai Y., Marcus M. A., Tamura N., Davis J. A. and Zachara J. M. (2007) Spectroscopic evidence for uranium bearing precipitates in vadose zone sediments at the Hanford 300-area site. *Environ. Sci. Technol.* **41**, 4633–4639.

Bildstein O. and Claret F. (2015) Chapter 5 – Stability of clay barriers under chemical perturbations. In *Natural and Engineered Clay Barriers, Developments in Clay Science* (eds. C. Tournassat, C. I. Steefel, I. C. Bourg and F. Bergaya). Elsevier, pp. 155–188.

Borisover M. and Davis J. A. (2015) Chapter 2 – Adsorption of inorganic and organic solutes by clay minerals. In *Natural and Engineered Clay Barriers, Developments in Clay Science* (eds. C. Tournassat, C. I. Steefel, I. C. Bourg and F. Bergaya). Elsevier, pp. 33–70.

Bourg I. C., Sposito G. and Bourg A. C. M. (2007) Modeling the acid-base surface chemistry of montmorillonite. *J. Colloid Interface Sci.* **312**, 297–310.

Bradbury M. H. and Baeyens B. (2003) Porewater chemistry in compacted re-saturated MX-80 bentonite. *J. Contam. Hydrol.* **61**, 329–338.

Bradbury M. H. and Baeyens B. (2005) Modelling the sorption of Mn(II), Co(II), Ni(II), Zn(II), Cd(II), Eu(III), Am(III), Sn(IV), Th(IV), Np(V) and U(VI) on montmorillonite: linear free energy relationships and estimates of surface binding constants for some selected heavy metals and actinides. *Geochim. Cosmochim. Acta* **69**, 875–892.

Bradbury M. H. and Baeyens B. (2011) Predictive sorption modelling of Ni(II), Co(II), Eu(IIII), Th(IV) and U(VI) on MX-80 bentonite and Opalinus Clay: A "bottom-up" approach. *Appl. Clay Sci.* **52**, 27–33.

Brigatti M. F., Galán E. and Theng B. K. G. (2013) Chapter 2 – Structure and mineralogy of clay minerals. In *Handbook of Clay Science, Developments in Clay Science* (eds. F. Bergaya and G. Lagaly). Elsevier, pp. 21–81.

Catalano J. G. and Brown, Jr., G. E. (2005) Uranyl adsorption onto montmorillonite: evaluation of binding sites and carbonate complexation. *Geochim. Cosmochim. Acta* **69**, 2995–3005.

Chang F. R. C. and Sposito G. (1994) The electrical double layer of a disked-shaped clay mineral particle: effect of particle size. *J. Colloid Interface Sci.* **163**, 19–27.

Chang F. R. C. and Sposito G. (1996) The electrical double layer of a disked-shaped clay mineral particle: effect of electrolyte properties and surface charge density. *J. Colloid Interface Sci.* **178**, 555–564.

Chisholm-Brause C., Conradson S. D., Buscher C. T., Eller P. G. and Morris D. E. (1994) Speciation of uranyl sorbed at multiple binding sites on montmorillonite. *Geochim. Cosmochim. Acta* **58**, 3625–3631.

Chisholm-Brause C. J., Berg J. M., Matzner R. A. and Morris D. E. (2001) Uranium (VI) sorption complexes on montmorillonite as a function of solution chemistry. *J. Colloid Interface Sci.* **233**, 38–49.

Choppin G. R. (2006) Actinide speciation in aquatic systems. *Mar. Chem.* **99**, 83–92.

Curtis G. P., Fox P., Kohler M. and Davis J. A. (2004) Comparison of in situ uranium K_D values with a laboratory determined surface complexation model. *Appl. Geochem.* **19**, 1643–1653.

Davis J. A., James R. O. and Leckie J. O. (1978) Surface ionization and complexation at the oxide/water interface: I. Computation of electrical double layer properties in simple electrolytes. *J. Colloid Interface Sci.* **63**, 480–499.

Davis J. A., Meece D. E., Kohler M. and Curtis G. P. (2004) Approaches to surface complexation modeling of Uranium(VI) adsorption on aquifer sediments. *Geochim. Cosmochim. Acta* **68**, 3621–3641.

Dent A. J., Ramsay J. D. and Swanton S. W. (1992) An EXAFS study of uranyl ion in solution and sorbed onto silica and montmorillonite clay colloids. *J. Colloid Interface Sci.* **150**, 45–60.

Duc M., Gaboriaud F. and Thomas F. (2005) Sensitivity of the acid-base properties of clays to the methods of preparation and measurement: 2. Evidence from continuous potentiometric titrations. *J. Colloid Interface Sci.* **289**, 148–156.

Fox P. M., Davis J. A. and Zachara J. M. (2006) The effect of calcium on aqueous uranium (VI) speciation and adsorption to ferrihydrite and quartz. *Geochim. Cosmochim. Acta* **70**, 1379–1387.

Gaboreau S., Claret F., Crouzet C., Giffaut E. and Tournassat C. (2012a) Caesium uptake by Callovian-Oxfordian clayrock under alkaline perturbation. *Appl. Geochem.* **27**, 1194–1201.

Gaboreau S., Lerouge C., Dewonck S., Linard Y., Bourbon X., Fialips C. I., Mazurier A., Pret D., Borschneck D., Montouillout V., Gaucher E. C. and Claret F. (2012b) In-situ interaction of cement paste and shotcrete with claystones in a deep disposal context. *Am. J. Sci.* **312**, 314–356.

Gaucher E. C. and Blanc P. (2006) Cement/clay interactions – a review: experiments, natural analogues, and modeling. *Waste Manage.* **26**, 776–788.

Geckeis H., Schäfer T., Hauser W., Rabung T., Missana T., Degueldre C., Möri A., Eikenberg J., Fierz T. and Alexander W. (2004) Results of the colloid and radionuclide retention experiment (CRR) at the Grimsel Test Site (GTS), Switzerland–impact of reaction kinetics and speciation on radionuclide migration. *Radiochimica Acta/Int. J. Chem. Aspects Nucl. Sci. Technol.* **92**, 765–774.

Giaquinta D., Soderholm L., Yuchs S. and Wasserman S. (1997) The speciation of uranium in a smectite clay: evidence for catalysed uranyl reduction. *Radiochim. Acta* **76**, 113–122.

Giffaut E., Grivé M., Blanc P., Vieillard P., Colàs E., Gailhanou H., Gaboreau S., Marty N., Madé B. and Duro L. (2014) Andra thermodynamic database for performance assessment: ThermoChimie. *Appl. Geochem.* **49**, 225–236.

Graham M. C., Oliver I. W., MacKenzie A. B., Ellam R. M. and Farmer J. G. (2011) Mechanisms controlling lateral and vertical porewater migration of depleted uranium (DU) at two UK weapons testing sites. *Sci. Total Environ.* **409**, 1854–1866.

Grawunder A., Lonschinski M., Merten D. and Büchel G. (2009) Distribution and bonding of residual contamination in glacial sediments at the former uranium mining leaching heap of Gessen/Thuringia, Germany. *Chemie der Erde-Geochemistry* **69**, 5–19.

Hartmann E., Baeyens B., Bradbury M. H., Geckeis H. and Stumpft T. (2008) A spectroscopic characterization and quantification of M(III)/clay mineral outer-sphere complexes. *Environ. Sci. Technol.* **42**, 7601–7606.

Hennig C., Reich T., Dähn R. and Scheidegger A. (2002) Structure of uranium sorption complexes at montmorillonite edge sites. *Radiochim. Acta* **90**, 653–657.

Hsi C. D. and Langmuir D. (1985) Adsorption of uranyl onto ferric oxyhydroxides: application of the surface complexation site-binding model. *Geochim. Cosmochim. Acta* **49**, 1931–1941.

Hursh J., and Spoor N. (1973) Data on man. In: Uranium· Plutonium Transplutonic Elements. pp. 197–239.

Hyun S. P., Cho Y. H., Hahn P. S. and Kim S. J. (2001) Sorption mechanism of U(VI) on a reference montmorillonite: binding to the internal and external surfaces. *J. Radioanal. Nucl. Chem.* **250**, 55–62.

Kowal-Fouchard A., Drot R., Simoni E. and Ehrhardt J. J. (2004) Use of spectroscopic techniques for uranium(VI)/montmorillonite interaction modeling. *Environ. Sci. Technol.* **38**, 1399–1407.

Liu X., Lu X., Sprik M., Cheng J., Meijer E. J. and Wang R. (2013) Acidity of edge surface sites of montmorillonite and kaolinite. *Geochim. Cosmochim. Acta* **117**, 180–190.

Liu X., Cheng J., Sprik M., Lu X. and Wang R. (2014) Surface acidity of 2:1-type dioctahedral clay minerals from first principles molecular dynamics simulations. *Geochim. Cosmochim. Acta* **140**, 410–417.

Liu X., Cheng J., Sprik M., Lu X. and Wang R. (2015a) Interfacial structures and acidity of edge surfaces of ferruginous smectites. *Geochim. Cosmochim. Acta* **168**, 293–301.

Liu X., Lu X., Cheng J., Sprik M. and Wang R. (2015b) Temperature dependence of interfacial structures and acidity of clay edge surfaces. *Geochim. Cosmochim. Acta* **160**, 91–99.

Marques Fernandes M., Baeyens B., Dähn R., Scheinost A. C. and Bradbury M. H. (2012) U(VI) sorption on montmorillonite in the absence and presence of carbonate: a macroscopic and microscopic study. *Geochim. Cosmochim. Acta* **93**, 262–277.

Marques Fernandes M., Ver N. and Baeyens B. (2015) Predicting the uptake of Cs Co, Ni, Eu, Th and U on argillaceous rocks using sorption models for illite. *Appl. Geochem.* **59**, 189–199.

McKinley J. P., Zachara J. M., Smith S. C. and Turner D. R. (1995) The influence of uranyl hydrolysis and multiple site-binding reactions on adsorption of U(VI) to montmorillonite. *Clays Clay Miner.* **43**, 586–598.

Meleshyn A., Azeroual M., Reeck T., Houben G., Riebe B. and Bunnenberg C. (2009) Influence of (calcium-) uranyl- carbonate complexation on U (VI) sorption on Ca-and Na-bentonites. *Environ. Sci. Technol.* **43**, 4896–4901.

Milodowski A. E., Norris S. and Alexander W. R. (2016) Minimal alteration of montmorillonite following long-term interaction with natural alkaline groundwater: implications for geological disposal of radioactive waste. *Appl. Geochem.* **66**, 184–197.

Missana T., Alonso U., García-Gutiérrez M. and Mingarro M. (2008) Role of bentonite colloids on europium and plutonium migration in a granite fracture. *Appl. Geochem.* **23**, 1484–1497.

Morris D. E., Chisholm-Brause C. J., Barr M. E., Conradson S. D. and Eller P. G. (1994) Optical spectroscopic studies of the sorption of UO22+ species on a reference smectite. *Geochim. Cosmochim. Acta* **58**, 3613–3623.

Muurinen A. and Lehikoinen J. (1999) Porewater chemistry in compacted bentonite. *Eng. Geol.* **54**, 207–214.

NIH (2016). U.S. National Library of Medicine, TOXMAP classic Environmental Health Maps: <http://toxmap-classic.nlm.nih.gov/toxmap/superfund/mapControls.do> (accessed on 05-24-2016).

Pabalan R. T. and Turner D. R. (1996) Uranium (6+) sorption on montmorillonite: experimental and surface complexation modeling study. *Aquat. Geochem.* **2**, 203–226.

Parkhurst D. L., and Appelo C. A. J. (1999). User's guide to PHREEQC (Version 2) – a computer program for speciation, batch-reaction, one-dimensional transport, and inverse geochemical calculations. Denver, CO. U.S. Geological Survey. Water resources investigations report 99–4259. 312 p.

Parkhurst D. L., and Appelo C. A. J. (2013) Description of input and examples for PHREEQC Version 3 – a computer program for speciation,batch-reaction, one-dimensional transport, and inverse geochemical calculations. U.S. Geological Survey Techniques and Methods, book 6, chap. A43, 497 p., available at <http://pubs.usgs.gov/tm/06/a43/>.

Savage D., Bateman K., Hill P., Hughes C., Milodowski A. E., Pearce J. M., Rae E. and Rochelle C. A. (1992) Rate and mechanism of the reaction of silicates with cement pore fluids. *Appl. Clay Sci.* **7**, 33–45.

Schäfer T., Geckeis H., Bouby M. and Fanghänel T. (2004) U, Th, Eu and colloid mobility in a granite fracture under near-natural flow conditions. *Radiochimica Acta/Int. J. Chem. Aspects of Nucl. Sci. Technol.* **92**, 731–737.

Schlegel M. L. and Descostes M. (2009) Uranium uptake by hectorite and montmorillonite: a solution chemistry and polarized EXAFS study. *Environ. Sci. Technol.* **43**, 8593–8598.

Secor R. B. and Radke C. J. (1985) Spillover of the diffuse double layer on montmorillonite particles. *J. Colloid Interface Sci.* **103**, 237–244.

Steefel C. I., Appelo C. A. J., Arora B., Jacques D., Kalbacher T., Kolditz O., Lagneau V., Lichtner P. C., Mayer K. U., Meeussen J. C. L., Molins S., Moulton D., Shao H., Šimunek J., Spycher N., Yabusaki S. B. and Yeh G. T. (2015) Reactive transport codes for subsurface environmental simulation. *Comput. Geosci.* **19**, 445–478.

Stumm, W., et al. (1992). Chemistry of the solid-water interface: processes at the mineral-water and particle-water interface in natural systems. John Wiley & Son Inc.

Sylwester E. R., Hudson E. A. and Allen P. G. (2000) The structure of uranium (VI) sorption complexes on silica, alumina, and montmorillonite. *Geochim. Cosmochim. Acta* **64**, 2431–2438.

Tinnacher R. M., Holmboe M., Tournassat C., Bourg I. C. and Davis J. A. (2016) Ion adsorption and diffusion in smectite: molecular, pore, and continuum scale views. *Geochim. Cosmochim. Acta* **177**, 130–149.

Tournassat C. and Appelo C. A. J. (2011) Modelling approaches for anion-exclusion in compacted Na-bentonite. *Geochim. Cosmochim. Acta* **75**, 3698–3710.

Tournassat C., Neaman A., Villiéras F., Bosbach D. and Charlet L. (2003) Nanomorphology of montmorillonite particles: estimation of the clay edge sorption site density by low-pressure gas adsorption and AFM observations. *Am. Miner.* **88**, 1989–1995.

Tournassat C., Bizi M., Braibant G. and Crouzet C. (2011) Influence of montmorillonite tactoid size on Na-Ca cation exchange reactions. *J. Colloid Interface Sci.* **364**, 443–454.

Tournassat C., Grangeon S., Leroy P. and Giffaut E. (2013) Modeling specific pH dependent sorption of divalent metals on montmorillonite surfaces. A review of pitfalls, recent achievements and current challenges. *Am. J. Sci.* **313**, 395–451.

Tournassat C., Bourg I. C., Steefel C. I. and Bergaya F. (2015a) Chapter 1 – Surface properties of clay minerals. In *Natural and Engineered Clay Barriers. Developments in Clay Science* (eds. C. Tournassat, C. I. Steefel, I. C. Bourg and F. Bergaya). Elsevier, pp. 5–31.

Tournassat C., Steefel C., Bourg I. and Bergaya F. (2015b) *Natural and Engineered Clay Barriers*. Elsevier.

Tournassat C., Vinsot A., Gaucher E. C. and Altmann S. (2015c) Chapter 3 – Chemical conditions in clay-rocks. In *Natural and Engineered Clay Barriers, Developments in Clay Science* (eds. C. Tournassat, C. I. Steefel, I. C. Bourg and F. Bergaya). Elsevier, pp. 71–100.

Tournassat C., Davis J. A., Chiaberge C., Grangeon S. and Bourg I. C. (2016a) Modeling the acid–base properties of montmorillonite edge surfaces. *Environ. Sci. Technol.* **50**, 13436–13445.

Tournassat C., Gaboreau S., Robinet J.-C., Bourg I. C. and Steefel C. I. (2016b) Impact of microstructure on anion exclusion in compacted clay media. *CMS Workshop Lecture Series* **21**, 137–149.

Tournassat C. and Steefel C. I. (2015) Ionic transport in nanoporous clays with consideration of electrostatic effects. *Rev. Mineral. Geochem.* **80**, 287–330.

Troyer L. D., Maillot F., Wang Z., Wang Z., Mehta V. S., Giammar D. E. and Catalano J. G. (2016) Effect of phosphate on U (VI) sorption to montmorillonite: ternary complexation and precipitation barriers. *Geochim. Cosmochim. Acta* **175**, 86–99.

Turner G. D., Zachara J. M., McKinley J. P. and Smith S. C. (1996) Surface-charge properties and UO_2^{2+} adsorption of a subsurface smectite. *Geochim. Cosmochim. Acta* **60**, 3399–3414.

U.S. Environmental Protection Agency (2001) Radionuclides Rule: A Quick Reference Guide. <http://nepis.epa.gov/Exe/ZyPDF.cgi?Dockey=30006644.txt> (accessed on 05-25-2016).

Van Olphen, H. (1992) Particle associations in clay suspensions and their rheological implications. In Clay-water interface and its rheological implications (eds. N. Güven, R.M. Pollastro). The Clay Minerals Society. pp. 191–210.

Villalobos M., Trotz M. A. and Leckie J. O. (2001) Surface complexation modeling of carbonate effects on the adsorption of Cr (VI), Pb (II), and U (VI) on goethite. *Environ. Sci. Technol.* **35**, 3849–3856.

Waite T. D., Davis J. A., Payne T. E., Waychunas G. A. and Xu N. (1994) Uranium (VI) adsorption to ferrihydrite: application of a surface complexation model. *Geochim. Cosmochim. Acta* **58**, 5465–5478.

Wersin P. (2003) Geochemical modelling of bentonite porewater in high-level waste repositories. *J. Contam. Hydrol.* **61**, 405–422.

Wersin P., Curti E. and Appelo C. A. J. (2004) Modelling bentonite–water interactions at high solid/liquid ratios: swelling and diffuse double layer effects. *Appl. Clay Sci.* **26**, 249–257.

White G. N. and Zelazny L. W. (1988) Analysis and implications of the edge structure of dioctahedral phyllosilicates. *Clays Clay Miner.* **36**, 141–146.

Wolthers M., Charlet L., and Tournassat C. (2006) Reactivity of bentonite. An additive model applied to uranyl sorption. In Surface complexation modelling (ed. J. Lützenkirchen). Elsevier.

World Health Organization (2004) Uranium in drinking-water: background document for development of WHO guidelines for drinking-water quality. WHO/SDE/WSH/03.04/118.

Associate editor: Annie B. Kersting